

Optimal Heat Extraction for Geothermal Energy Applications

THESIS

Presented in Partial Fulfillment of the Requirements for the Degree Master of Science in
the Graduate School of The Ohio State University

By

Iti Harshad Patel

Graduate Program in Civil Engineering

The Ohio State University

2016

Master's Examination Committee:

Professor Jeffrey Bielicki, Advisor

Professor Ethan Kubatko

Professor Sathya Gopalakrishnan

Copyright by
Iti Harshad Patel
2016

Abstract

Sedimentary basins are emerging candidates for geothermal deployment due to their widespread presence in the subsurface, large storage capacity, and high temperatures. These geothermal systems rely on the temperature of the reservoir—and thus the temperature of the extraction fluid produced to the surface—but these temperatures can decrease if the rate at which heat is extracted from the reservoir exceeds the rate at which the natural geothermal heat flux increases the temperature. In this context, sustainability is often synonymous with extracting heat at a rate that maintains the temperature of the production fluid at a desired level. This perspective of sustainability focuses on the physical/environmental performance of the geothermal reservoir. But preserving heat in the reservoir may not be economically viable. Environmental and economic performance are interconnected, and systems must consider both of these metrics when determining an optimal operation strategy to conserve both the longevity of the resource and the associated economic profit. Natural resource economics focuses on developing strategies for resource management and/or allocation that weighs the environmental and economic benefits of a system.

The following thesis presents a natural resource economics model for the optimal management of a geothermal resource using conventionally used water or carbon dioxide

(CO₂) as a heat extraction fluid. I investigated the performance of a sedimentary basin geothermal resource under a variety of scenarios, parameterized those results to accurately predict change in geothermal performance, and implemented those results in a natural resource economic model. The Non-isothermal Unsaturated- saturated Flow and Transport (NUFT) code simulates a sedimentary basin geothermal reservoir under a range of geologic conditions and was used to understand and parameterize geothermal performance. I combined the simulation outputs from all the scenarios by normalizing the production temperature and energy that is extracted to create a reduced form representation of this relationship. This reduced form serves as an input into the natural resource economic model that uses Microsoft Excel's Optimization Solver to determine the optimal mass flowrate time path to extract heat given the profit that can be made and the natural rate at which the reservoir temperature renews.

The reservoir simulation results show that the relationship between normalized temperature of the produced fluid and normalized energy that is extracted is the Richard's curve (i.e. a generalized logistic curve). The regeneration rate of the reservoir, the rate at which temperature renews within a reservoir, is considerably smaller than the rate of economic growth. As such, results from the natural resource economic model suggest it is often optimal to drawdown the temperature of the reservoir to gain the quickest payback of investment.

Because of God,

Because of my parents, Harshad and Mina Patel, on whose shoulders I stand,

Because of my brother, Chintan Patel, who teaches me that no difficulty is too big to face as long as you have self-confidence,

Because of my sister, Meghna Patel, who sees the best in me even (and especially) when I am at my worst,

Because of my brother, Darshit Gandhi, who makes having integrity look straightforward and effortless,

Because of my sister, Sweta Gandhi, who refuses to let go of me when I so frequently shut out the world,

Because of my nephew, Nimitt Patel, who loves simply, without expectations or pride,

And because of my nephew, Aadarsh Gandhi, who brought tears of happiness to my eyes (twice),

I am. Thank you.

Acknowledgements

My first, and deepest gratitude to my advisor, Professor Jeffrey Bielicki, who has consistently and diligently pushed me to be a better student, researcher, engineer, writer, and human being. Without his guidance, these two years would have been impossible. But more than his guidance in my work, I want to thank him for his ability to constantly push me out of my comfort zone and continue the never-ending process of learning.

Thank you to the National Science Foundation (NSF) Sustainable Energy Pathways program (1230691) for the funding they provided.

Thank you to my committee members, Professor Ethan Kubatko and Professor Sathya Gopalakrishnan, for being such great teachers. It is rare to find teachers who both inspire you to learn and guide you along the way.

Thank you to Lawrence Livermore National Lab, and specifically to Dr. Tom Buscheck and Dr. Yunwei Sun, for the unique opportunities and support they provided in learning the NUFT code.

Thank you to all the members of the Energy Sustainability Lab, Jonathan Ogland-Hand, Julie Langenfeld, Glenn Sutula, Kelsey Hunter, Paige Hagley, and Yaoping Wang, for the

patience, feedback, motivation, and company you gave these past two years. I will forever remember the hours we spent in solid work, the hours we spent in laughter, and the hours we spent in mutual distress. Thank you for being my weekday family (and sometimes my weekend, holidays, and most evenings family).

Thank you to Pandurang Shastri Athavale, my life teacher and friend.

Finally, to my friends, who have all heard me stress, whine, and cry about school. Thank you for filling me with strength and confidence over, and over, and over again. Thank you Dolly Patel, Bansri Ribadiya, Zil Gandhi, Vaidehi Shah, Madhavi Bhavsar, Shrie Dave, Brinda Dave, Dr. Vimal and Prerna Desai, Jay Patel, Neeli Oza, Kishan Patel, Ravi Patel, and lastly thank you to Book Club for making my life more difficult.

Vita

May 2009Hilliard Darby High School

December 2013B.S. Environmental Engineering The Ohio
State University

Spring 2015, 2016Graduate Teaching Associate, Department
of Civil Engineering, The Ohio State
University

August 2014 - presentM.S. Civil, Environmental and Geodetic
Engineering, The Ohio State University

Publications

Patel, I.H., Bielicki, J.M., Buscheck, T.A., 2016. A Reduced Form Representation of Temperature Drawdown in Sedimentary Basin Geothermal Reservoirs for the Development of Optimal Management Strategies, in: 41st Stanford Geothermal Workshop. Stanford, California, pp. 1–7.

Fields of Study

Major Field: Civil Engineering – Energy Sustainability

Table of Contents

Abstract	ii
Acknowledgements	v
Vita	vii
List of Tables	xi
List of Figures	xii
Chapter 1: Geothermal Energy Background	1
The Global Energy Challenge	1
Geothermal Energy Resources	3
Sedimentary Basin Geothermal Energy	6
Geothermal Renewability and Sustainability	7
Natural Resource Economics	10
Conceptual Analogies.....	10
Natural Resource Economics Model	11
Overview of Methodology	12
The Nature of Computer Models	13
Chapter 2: Reservoir Modeling Using NUFT Simulation	15

NUFT Code	15
Description of Simulation Reservoir	16
Reservoir Parameters	18
Fluid Parameters	19
Solution Parameters	22
Chapter 3: Processing Simulation Results	24
Generalized Logistic Curve	24
Data Normalization	26
Regeneration of Heat in the Reservoir	28
Chapter 4: Dynamic Optimization Model	39
Description of Model Objective	39
Decision and State Variables	41
Input, Output, and Fixed Parameters	43
Solution Method	45
Chapter 5: Results	46
Geothermal Reservoir Performance	46
CO ₂ Fluid Production	48
Comparing Temperature Drawdown of Water and CO ₂	51
Normalization Results	52

Comparison of Normalization Results using NUFT Data and STATA Regression	58
Optimal Operation of a Geothermal Reservoir	59
Chapter 6: Future Research and Conclusion	64
Suggestions for Further Research	64
Conclusion.....	67
References	68
Appendix A: Nomenclature	78
Appendix B: Programming Code	81

List of Tables

Table 1: Reservoir Parameters	19
Table 2: Mass Flowrate Specifications for CO ₂ and water for Each Permeability; *for CO ₂ only.....	21
Table 3: NUFT Output Variable Tolerances	23
Table 4: Average Specific Heat Capacity in Isobaric Conditions	25
Table 5: STATA Regression Results for Heat Flow into Reservoir for Water and CO ₂ ..	36
Table 6: Input Parameters of Natural Resource Economic Model	44
Table 7: Output Parameters of Optimal Path	44
Table 8: Coefficients of the Logistic Curve Fit to the Normalized Temperature and Heat Extraction Data Using Water	53
Table 9: Coefficients of the Logistic Curve Fit to the Normalized Temperature and Heat Extraction Data Using CO ₂	55
Table 10: Input Parameters Used for Following Results Unless Specified Otherwise.....	60

List of Figures

Figure 1: Percent of Total United States Electricity Consumption (Source: Institute of Energy Research)	3
Figure 2: Abbreviated Taxonomy of Geothermal Energy Resources.....	5
Figure 3: A Schematic of Sustainable Geothermal Production Presented by Axelsson et al. (2004).....	9
Figure 4: Overview of Methodology	13
Figure 5: Model of the Radial Well System Used in this Study.....	17
Figure 6: Reservoir Animation of a CO ₂ -Plume within a Reservoir Highlighting Heat Transfer Processes	30
Figure 7: (a) Schematic of Reservoir Cells and (b) Example of Heat Flow into Reservoir for Simulation using Water with Parameters: Permeability(κ) = 10^{-13} m ² , Depth(z) = 2,500m, Temperature Gradient(G) = 50°C/km, Thickness(Δz) = 100m, Mass Flowrate(m) = 200 kg/s.....	32
Figure 8: Heat flow into Reservoir for Water and CO ₂ using a Mass Flowrate of 100 kg/s and 250 kg/s with Parameters: Permeability(κ) = 10^{-11} m ² , Depth(z) = 3,500m, Temperature Gradient(G) = 35°C/km, and Thickness(Δz) = 100m.....	34
Figure 9: Change in Temperature of Produced Fluid over Time for Different Permeabilities with Parameters: Depth(z) = 5,000m, Temperature Gradient(G) = 50°C/km, Thickness(Δz) = 100m, and Mass Flowrate(m) = 100 kg/s	37

Figure 10: Example Reservoir Simulations Results Using Water from NUFT with Parameters: Permeability(κ) = 10^{-11} m², Depth(z) = 3,500m, Temperature Gradient(G) = 35°C/km, Thickness(Δz) = 100m, and (a) Varying Mass Flowrate and (b) Mass Flowrate(m) = 100 kg/s 47

Figure 11: Breakthrough Time for Varying Mass Flowrates with Parameters: Permeability(κ) = 10^{-13} m², Depth(z) = 2,500m, Temperature Gradient(G) = 35°C/km, Thickness(Δz) = 100m, and Average Mole Fraction of CO₂ in the Production Well at Breakthrough Time: 0.09 49

Figure 12: Example of (a) CO₂ Breakthrough and (b) 99% Mole Fraction of CO₂ at Production Well with Parameters: Permeability(κ) = 10^{-11} m², Depth(z) = 3,500m, Temperature Gradient(G) = 35°C/km, Thickness(Δz) = 100m, and Mass Flowrate(m) = 100 kg/s 50

Figure 13: Temperature Drawdown in the Reservoir Using Water and CO₂ with Parameters: Permeability(κ) = 10^{-12} m², Depth(z) = 5,000m, Temperature Gradient(G) = 50°C/km, Thickness(Δz) = 100m, and Mass Flowrate(m) = 100 kg/s 51

Figure 14: Normalization of the Temperature of the Production Fluid as a Function of the Energy that is Extracted from the Reservoir for NUFT Simulations Using Water 53

Figure 15: Normalization of the Temperature of the Production Fluid as a Function of the Energy that is Extracted from the Reservoir for NUFT Simulations Using CO₂ 54

Figure 16: Normalization of the Temperature of the Production Fluid as a Function of the Energy that is Extracted from the Reservoir for NUFT Simulations Using CO₂ Parted by

Permeability (κ): $1 \times 10^{-11} \text{ m}^2$ (79 Simulations), $1 \times 10^{-12} \text{ m}^2$ (77 Simulations), $1 \times 10^{-13} \text{ m}^2$ (72 Simulations)	56
Figure 17: Normalization of the Temperature of the Production Fluid as a Function of the Energy that is Extracted from the Reservoir for NUFT Simulations Using CO ₂ Parted by Mass Flowrate (m): 100 kg/s (39 Simulations), 150 kg/s (34 Simulations), 200 kg/s (34 Simulations), 250 kg/s (33 Simulations).....	56
Figure 18: Normalization of the Temperature of the Production Fluid (Water and CO ₂) as a Function of the Energy that is Extracted from the Reservoir for NUFT Simulations Using STATA Regression	59
Figure 19: Optimal Mass Flowrate Time Path for Water using the Natural Resource Economics Model with Parameters: Permeability (κ) = 10^{-13} m^2 , Depth (z) = 3,500m, Temperature Gradient (G) = 35°C/km, and Thickness (Δz) = 100m.....	61
Figure 20: Economic Benefits and Cost Multiplier for Water using the Natural Resource Economics Model with Parameters: Permeability (κ) = 10^{-13} m^2 , Depth (z) = 3,500m, Temperature Gradient (G) = 35°C/km, and Thickness (Δz) = 100m	61
Figure 21: Optimal Mass Flowrate Time Path for CO ₂ using the Natural Resource Economics Model with Parameters: Permeability (κ) = 10^{-13} m^2 , Depth (z) = 3,500m, Temperature Gradient (G) = 35°C/km, and Thickness (Δz) = 100m	62
Figure 22: Economic Benefits and Cost Multiplier for CO ₂ using the Natural Resource Economics Model with Parameters: Permeability (κ) = 10^{-13} m^2 , Depth (z) = 3,500m, Temperature Gradient (G) = 35°C/km, and Thickness (Δz) = 100m	62

Chapter 1: Geothermal Energy Background

This chapter discusses the global energy challenge addressed by the use of geothermal energy, an alternative to non-renewable resources that can exacerbate global climate change. An inherent shortcoming of geothermal energy is the decrease in temperature of the produced fluid over time if the rate of extraction exceeds the rate of renewability. As such, a sustainable heat extraction management strategy should consider both environmental and economic performance of geothermal energy. Natural resource economics provides the approach for determining such a strategy.

The Global Energy Challenge

The global energy challenge is to mitigate the effects of climate change caused by heat-trapping gases that are released into the atmosphere such as carbon dioxide (CO₂) and methane, primarily through the burning of non-renewable energy sources (e.g. coal, petroleum, and oil). As of 2014, the global average temperature had increased by 0.69°C (1.24°F) above the 20th century average of 13.9°C (59.0°F) (NOAA National Centers for Environmental Information, 2015). The global temperature is expected to continue increasing unless drastic measures are not taken. Research on climate change surfaced in the late nineteenth century (Sawyer, 1972), but it was not until recently that national governments, the energy sector, and the general public took initiative to alleviate its on-set

(Bolin, 2007). These initiatives ranged from carbon taxes and new fuel economy standards to campaigns that encourage citizen-level effort to use alternative energy sources and individual consciousness of energy use (de Moor, 2001; Walker, 1995). For example, in December 2015, countries gathered in Paris France and decided to take initiatives that will maintain the global temperature change below 2°C (United Nations, 2015). The United States will need to make drastic changes in the sources of energy used if the country is to materialize this vision.

Emission reductions in the United States will occur when there is a shift in energy dependency from fossil fuels to sources with little to no greenhouse gas emissions (Figure 1). Nuclear energy is a “cleaner” source of energy with lifecycle emissions ranging from 30 to 60 grams CO₂/kWh (Sovacool, 2008). But, the radioactive waste associated with nuclear energy is highly hazardous and difficult to dispose of due to potential harmful health effects (Bowman et al., 1992; Ewing et al., 1995). Other renewable energy resources that are used to produce electricity—namely wind and solar—are inherently variable and naturally fluctuate throughout the day, season, and year. In contrast, the operator of a geothermal energy facility can control the rate at which heat is extracted because the geothermal heat flux does not vary, providing flexibility in energy supply that can match the oscillations in energy demand. A shift in the sources of energy currently used will require extensive research to improve and increase the energy conversion efficiency of renewable resources. Until the specific limitations surrounding renewable energy sources

are not addressed, renewable energy will not be able to replace the current dependency on non-renewable energy.

Geothermal Energy Resources

Geothermal energy is the use of heat found within the earth's crust. The use of geothermal energy has increased over the last decade, yet, as Figure 1 shows, makes up only 0.4% of the total United States electricity generation as of March 2015 (Bertani, 2012; Institute for Energy Reserach, 2015).

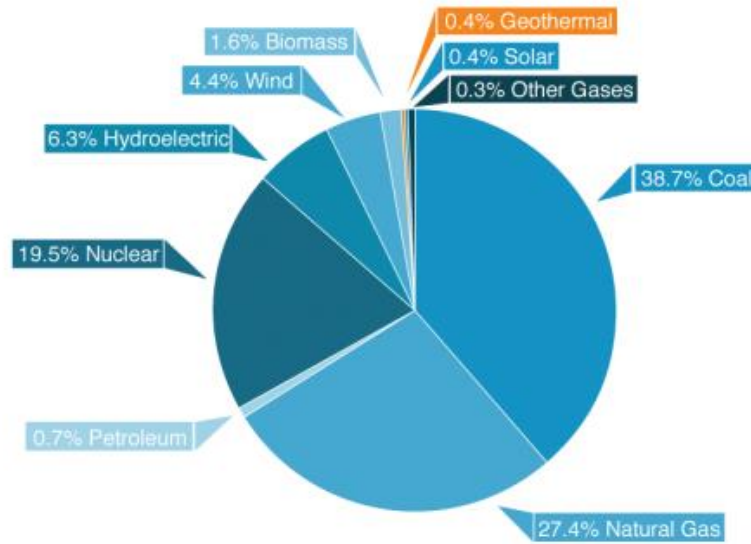


Figure 1: Percent of Total United States Electricity Consumption (Source: Institute of Energy Research)

This is a small use of the approximated 10^{13} EJ stored within the earth's subsurface (Rybach, 2007). To put this magnitude into perspective, it would take over 10^9 years of relying solely on geothermal energy to meet the world's energy demand to fully cool down

the earth (Rybach, 2007). Even if this is limited to the amount of energy in the upper five kilometers of the crust, there is still approximately 1.4×10^8 EJ of energy available for use (WEC, 1998). The source of this energy is the molten metal within the earth's core and the steady exothermic decay of radioactive material because of which there is a constant heat flux moving through the earth, making geothermal energy a renewable resource. As such, the temperature of the ground increases as you move deeper into the earth.

Depending on the temperature of the resource, geothermal energy can be used directly or indirectly (i.e. for electricity production). A condensed overview of geothermal energy is presented in Figure 2. This list is by no means exhaustive and is explicit to relevant geothermal resource types. Direct use of geothermal energy is extracted from shallow resources, with depths of 50m to 100m, and often intermediate resources, with depths of 100m to four kilometers (Olasolo et al., 2016). Direct-use geothermal energy using heat exchangers is used for heating and cooling purposes, such as district heating, greenhouses, swimming pools, industrial use, and agricultural use. Directly harnessing geothermal energy, from geysers for example, has been a long-standing practice worldwide, and thus, these low to intermediate temperature resource systems have been more extensively implemented compared to indirect use of geothermal energy. Particularly, there was a 43% increase in direct geothermal use from 1999 to 2004 (Fridleifsson et al., 2008). Nonetheless, indirect use of geothermal energy has proven to be a reliable resource for the generation of electricity (Arslan, 2010; Franco and Vaccaro, 2012; Kose, 2007). Many systems have emerged to extract deep, high-temperature geothermal energy, including

conventional hydrothermal systems, enhanced geothermal systems (EGS), and sedimentary basin geothermal energy systems.

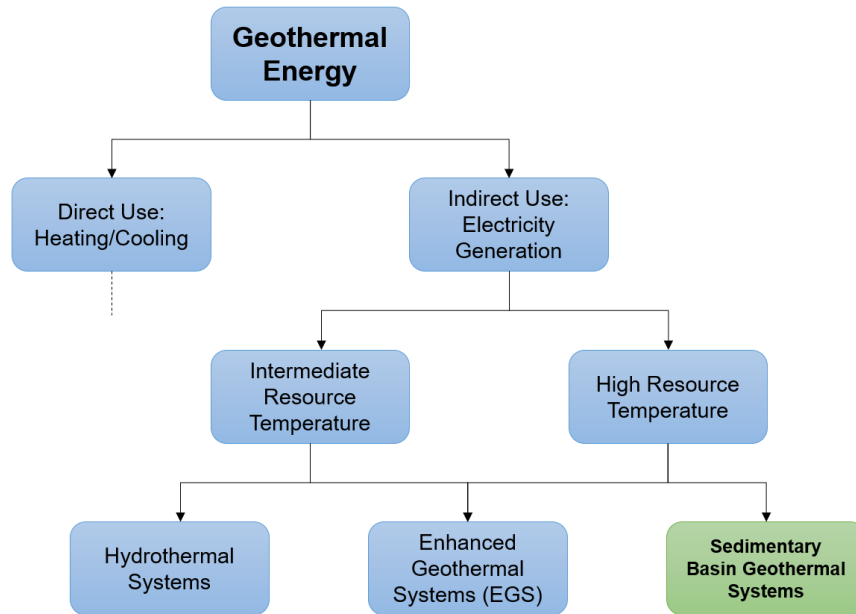


Figure 2: Abbreviated Taxonomy of Geothermal Energy Resources

Conventional hydrothermal energy systems use water in liquid or vapor form to extract heat from faults and fractures. While it can be implemented as a direct heating source, hydrothermal energy can be used for electricity generation under the appropriate conditions. Such conditions are commonly found near volcanic activity, tectonic plate boundaries, or hot spot anomalies (Goldstein et al., 2011). This makes hydrothermal energy for the purpose of electricity generation geographically limited.

The development of EGS was a successful attempt to expand the geographic application of geothermal energy by making use of impervious formations in the subsurface. The system fractures impermeable rock to create artificial permeability (Sanyal et al., 2007). EGS, like hydrothermal systems, also use water as the working fluid, though researchers are considering CO₂ for a variety of added benefits including CO₂ sequestration (Olasolo et al., 2016; Xu et al., 2015). Unlike hydrothermal, EGS systems are predominantly used for electricity generation. While the system is efficient in terms of energy extraction, the large drilling and fracturing costs of EGS make commercial implementation economically risky (Johnston et al., 2011).

Sedimentary Basin Geothermal Energy

Sedimentary basins are emerging as candidates for geothermal deployment using water or combining CO₂ sequestration and geothermal heat extraction in a CO₂ capture, utilization, and storage (CCUS) application (Cacace et al., 2010; Fridleifsson et al., 2008; Randolph and Saar, 2011). Compared to EGS resources, sedimentary basins have a widespread presence in the subsurface, large storage capacity, high temperatures, and natural permeability. These basins are generally filled with brine, and the depth ranges from one to six kilometers (Anderson, 2013). The general process of obtaining geothermal energy from a sedimentary basin consists of injecting a cold fluid, allowing the fluid to flow through the naturally porous and permeable reservoir. Heat transfer between the fluid and subsurface takes place, and hot fluid is produced from a nearby production well. Several processes in the power plant remove the heat from the produced fluid and the now cold

fluid is reinjected into the reservoir to repeat the heat extraction process. The discounted sum of net revenue from electricity generation must be larger than the high initial costs associated with geothermal energy for electricity production from the building of power plants for the system to be economically viable. This concept is significant in decision-making and policy as it considers the perspective of multiple stake-holders and disciplines.

Geothermal Renewability and Sustainability

An innate shortcoming of geothermal energy is the potential temperature decrease of produced fluid over time if the rate of energy that is extracted is greater than the natural rate at which temperature renews due to the constant heat flux of the earth. Temperature drawdown can be seen geothermal projects over time (e.g. Nesjavellir, Iceland reservoir, Olkaria, Kenya reservoir, Wairakei-Tauhara system), particularly where one resource is being tapped by multiple users (O’Sullivan et al., 2010; Rybach et al., 2000). For this reason, there was initially debate as to whether geothermal energy can be considered a renewable resource (Ledingham, 1998). After further inquiry, researchers determined geothermal energy is renewable because it renews on a societal time scale rather than a geologic one. Renewability is a property that describes the nature of the resource. But, the decreasing temperature of the produced fluid is a question of sustainability, an idea that describes how to use the resource (Stefansson, 2000). The concept of sustainability and sustainable development has evolved significantly from its original definition presented by the Brundtland Commission that defined it as “development that meets the needs of the present without compromising the ability of future generations to meet their own needs”

(Brundtland Commission, 1987). Sustainability is most commonly viewed as integrating three pillars: social, economic, and environmental. Again, this definition begets further questions as what factors each of these pillars consists of. The ambiguity of this definition has led to research that defines sustainability in a more explicit way and for specific applications.

According to Axelsson et al. (2004), sustainable production of a geothermal heat consists of extracting heat at the same rate as heat renewal to maintain a consistent level of production for a long time (Axelsson et al., 2004; Bromley et al., 2006). Figure 3 is a theoretical schematic of this idea. There is an optimal level of production that is sustainable for an indefinite amount of time. Energy production above this level is excessive and will cause temperature drawdown. Energy production below this level is underutilization of the resource.

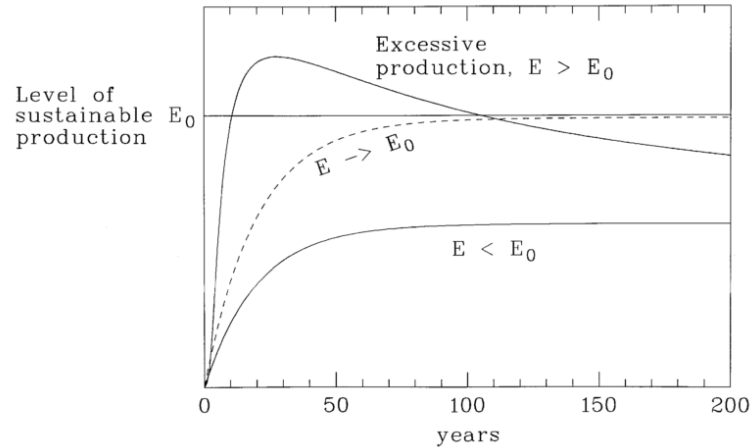


Figure 3: A Schematic of Sustainable Geothermal Production Presented by Axelsson et al. (2004)

The rate of renewability is important to consider from an environmental perspective, particularly in sensitive systems such as a fishery where overexploitation leads to crashes in the population and ultimately extinction. Yet, pure application of environmental sustainability can create market inefficiency by restricting the economic gain of that resource. On the other hand, deployment of geothermal systems requires the business to be profitable. There is a large financial risk associated with the geothermal business because of the large initial costs of building a power plant and drilling wells associated with geothermal energy for electricity generation. A fast return on investment can reduce this risk and give financial success for the owner this system (Murphy and Niitsuma, 1999). Both these perspectives suggest contrasting management strategies. While increasing the rate of extraction yields faster profit, this also means depletion of the resource itself. Such a management strategy limits the longevity of the system and, in the long run, can even

hinder future profit. As such, there is an inherent trade-off between environmental and economic sustainability, both of which need to be considered. An optimal management strategy then requires maximizing the value of selling heat subject to changes in the magnitude of heat that is extracted.

Natural Resource Economics

Natural resource economics is an integrated approach to resource management that considers the interaction between environmental processes, most often with reduced form representations, and economics. Examples include mining, fishery, and forestry, all of which have been used to describe geothermal energy.

Conceptual Analogies

Many researchers have used analogies of other resources or processes to describe an aspect of geothermal energy. Heat mining in a geothermal system is a common term used in the field because it captures the idea of extracting a valuable resource from within the subsurface of the earth (Fox et al., 2013; Xu et al., 2015). This analogy can be misleading in that a mining process refers to the extraction of a nonrenewable resource such as coal or ore. A comparison is made between geothermal heat and fish stocks in terms of renewability (Fridleifsson et al., 2008; Rybach, 2003; Stefansson, 2000). Fish populations decrease in size if the rate of fish harvest exceeds the natural population growth rate. Natural resource economic models for fishery determine an optimal path of extraction of fish by balancing the natural regeneration of fish stocks that are not harvested with the

profit from the sale of the fish that are harvested. Yet, the time-scale of regeneration of geothermal heat more closely imitates the growth of timber (Lei and Zhang, 2004; Sanyal, 2005). These approaches have been extensively studied for managing natural resources, such as fisheries and forests (Bonfil, 2005; Weitzman, 2003), but a natural resource economic approach has never been applied to determine a management strategy for geothermal heat extraction that I am aware of.

Natural Resource Economics Model

Natural resource economics typically uses extensions of calculus of variations, namely the Lagrangian or Hamiltonian methods, to solve resource allocation and optimization problems for a variety of problem types, including discrete time, continuous time, finite time horizons, and infinite time horizons (Conrad, 1999). These analytical solutions provide insight into the economic mechanisms of the system in question. But, calculus of variations follows the narrow formulation rules of unconstrained optimization. An alternative formulation and solution method has gained ground. Optimal control theory, a generalized version of calculus of variations, covers a wider range of applications in business, physics, and resource management because of its ability to be formulated for constraints and controls (Weitzman, 2003). Both calculus of variations and optimal control theory have been applied to the resource management of fisheries and forests (Gordon, 1954; Mitra and Wan, 1986; Tahvonen et al., 2010).

Overview of Methodology

The presented model applies the natural resource economic approach to a sedimentary basin geothermal resource used for electricity generation. Reservoir modeling simulates geothermal heat extraction to investigate the performance of the reservoir in terms of temperature of the produced fluid (Chapter 2 and 3). Subsequently, the results are processed to develop a reduced-form representation of heat flow into the reservoir and temperature drawdown of the produced fluid. The natural resource economic model in Chapter 4 uses this representation to determine the optimal heat extraction strategy that will maximize present value of benefits over time (Figure 4). The results of both are discussed in the final chapter, Chapter 5.

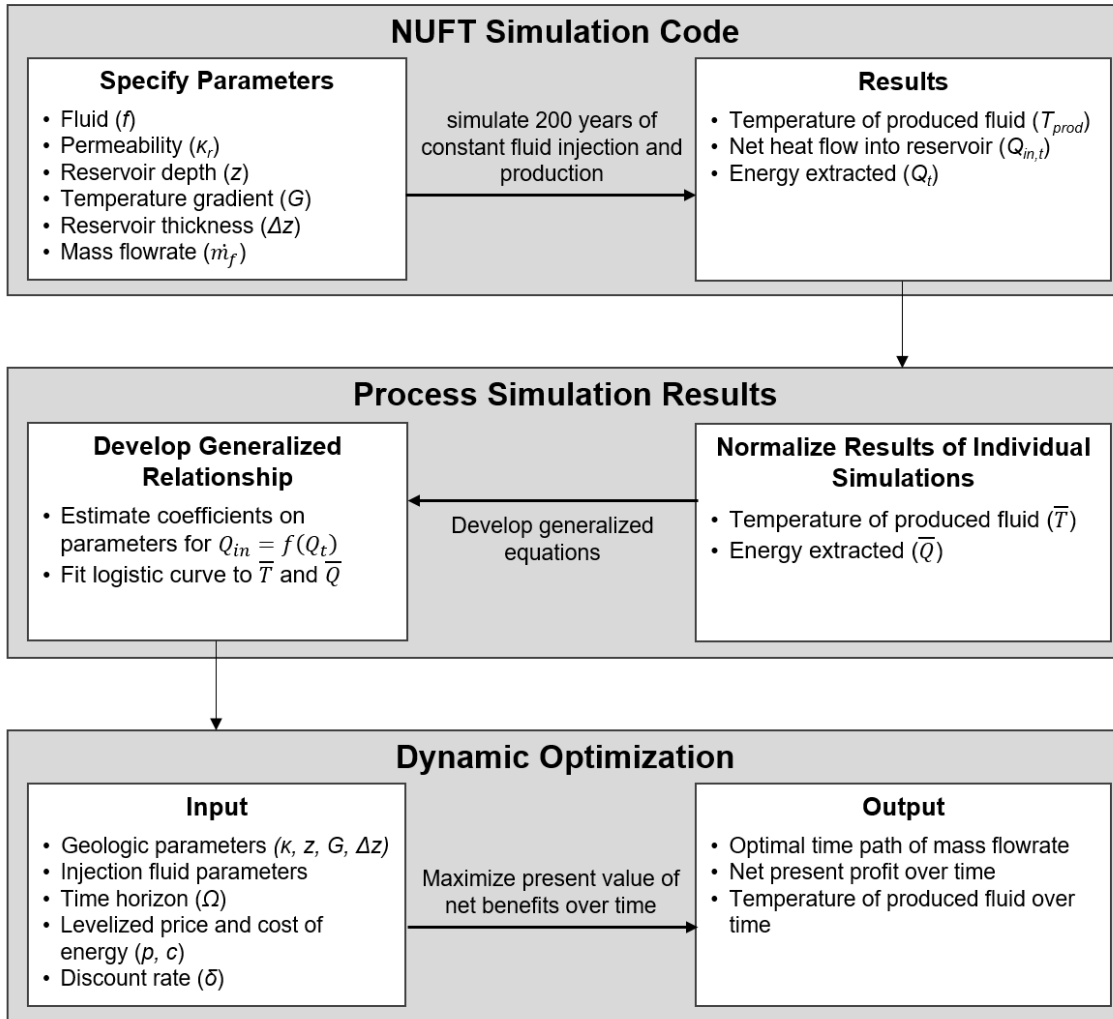


Figure 4: Overview of Methodology

The Nature of Computer Models

Computer models are substitutes for highly complex real world systems. Computer programming and modeling offers a simplified and interactive version of reality to develop intuition on how individuals and processes of a system interact, and, moreover, on how to best manage these systems (Sterman, 2000). They are tools that can be used to model across

time, space, and even between disciplines, such as the environment and the economy. This model can clarify the nature of trade-offs made between present/future value of profit/natural capital to operators and policy-makers. This is the motivation for developing the presented model. But, like with any model, assumptions and simplification are made because it is impossible to capture every aspect of a real system. Modeling in this sense is an iterative process that builds a model through slowly adding layers of complexity (Ford, 2010). As such, it is important to remember that the model presented in the next few chapters has made many assumptions in part because it is interdisciplinary. Each part of the model has the potential to be further explored to better capture the performance of geothermal heat during extraction.

Chapter 2: Reservoir Modeling Using NUFT Simulation

This chapter discusses the role of subsurface simulation in order to develop a reduced form representation of temperature drawdown in sedimentary basin geothermal reservoirs. The NUFT code simulates the performance of a sedimentary basin geothermal reservoir under a variety of geothermal conditions and operational scenarios using an R-z well configuration for the injection and production of water and supercritical CO₂.

NUFT Code

The Non-isothermal Unsaturated-saturated Flow and Transport (NUFT) code, created by Lawrence Livermore National Laboratory, simulates the flow and transport of multiphase, multicomponent fluids in porous media (Hao et al., 2011). NUFT integrates the finite difference method, spatial discretization, and the Newton-Raphson method to solve the conservation of mass and energy equations for each element of the mesh at each time step for output variables such as pressure, temperature, and concentration. The code contains distinct modules for (a) unconfined/confined flow, (b) single phase unsaturated flow, (c) single component unsaturated flow, and (d) multi-phase, multi-component flow with a thermal option (Nitao and Sun, 2015). The NUFT simulations use option (d) to have fluid parameters that vary with temperature and examine the changes in temperature during geothermal heat extraction.

This model has been used to examine the performance of subsurface reservoirs for nuclear waste disposal, CO₂ storage in sedimentary basins, groundwater remediation, and enhanced petroleum recovery (Buscheck et al., 2003; Johnson et al., 2005; Mansoor et al., 2015; Nitao and Sun, 2015; Recharad et al., 2014; Sahni et al., 2000; Sun et al., 2000). NUFT has been tested for field validation of groundwater remediation, particularly using soil-vapor extraction (Nitao et al., 2000). Similarly, NUFT has extensively been applied to examine radioactive waste disposal and waste container degradation in Yucca Mountain to the point of complete failure due to thermal and chemical processes (Recharad et al., 2014). As such, this work uses the NUFT code to study temperature drawdown during geothermal heat extraction under different geologic and operational scenarios.

Description of Simulation Reservoir

I implemented a two dimensional, cylindrical mesh in NUFT. The radially symmetric R-z model contains a vertical column of elements that represent a perforated central injection well and an element that represents a perforated radial production well (Figure 5). The injection well and the production well are separated by a radial distance of 700m. Similar R-z configurations have been used in previous modeling studies that simulate the performance of sedimentary basin geothermal reservoirs (Adams et al., 2015, 2014; Garapati et al., 2015, 2014b; Saar et al., 2015). The injection well covers the thickness of the reservoir with a radius of 0.5m. The production well has a length of five meters from

the top of the reservoir and has a width of 0.5m as seen in Figure 5. The reservoir was divided into 23 radial cells and 11 vertical cells.

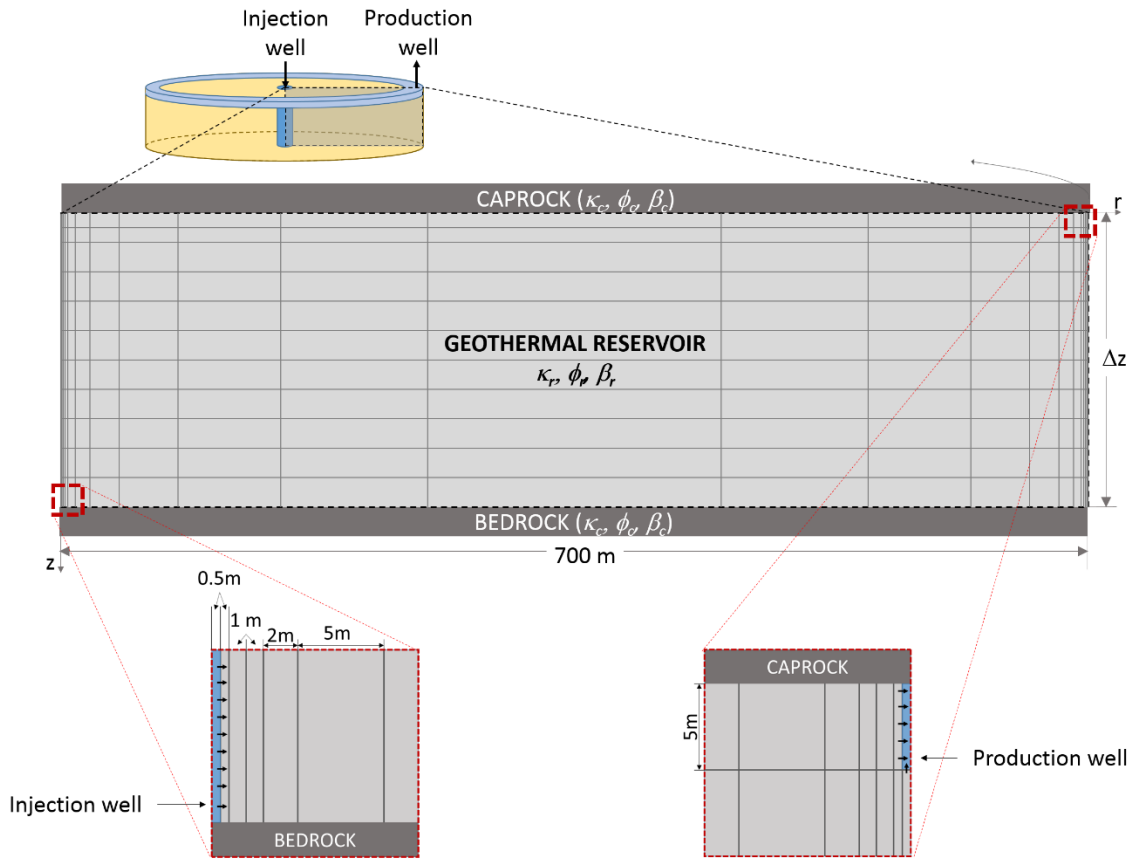


Figure 5: Model of the Radial Well System Used in this Study

The porous and permeable reservoir was modeled as a laterally unconfined aquifer, with the mesh extending out to approximately 82,000m beyond the reservoir. The reservoir is vertically confined by an impervious caprock above the reservoir and an impervious bedrock below the reservoir, with the basement 4,000m below the reservoir. The basement is 6,600m below the surface. The properties of the caprock and bedrock are similar to typical sandstones and have been used in previous papers that investigated CO₂ injection

into deep saline aquifers for sequestration from the atmosphere and for geothermal energy production using CO₂ and native brine (Table 1) (Birkholzer et al., 2009; Buscheck et al., 2013). Figure 5 shows a model of radial well system used in this study, where the element mesh is to scale.

Each simulation used a distinct combination of fluid, depth to the top of the reservoir, reservoir thickness, reservoir permeability, geothermal temperature gradient, and mass flowrate (Table 1 and Table 2). The parameters chosen for the simulations cover a range of the characteristics of sedimentary basins in the United States, and have been investigated in previous studies of sedimentary basin geothermal energy production and CO₂ storage (Anderson, 2013; Cacace et al., 2010).

Reservoir Parameters

The mass flowrate of the injection well was set equal to the mass flowrate of the production well in every scenario to allow the analysis to focus on the temperature of the produced fluid as the primary determinant of the use of the geothermal resource as opposed to pressure. Moreover, equalizing injection and production mass flowrates avoids potential geo-mechanical effects from overpressure (Garapati et al., 2014a; Holloway, 2005). The physical parameters for the reservoir and the confining unit for the scenarios simulated in NUFT are provided in Table 1.

Table 1: Reservoir Parameters

Parameter	Parameter Value
Permeability [m^2]:	
<i>Reservoir, κ_r</i>	$10^{-11}, 10^{-12}, 10^{-13}, 5 \times 10^{-14}, 10^{-14}, 5 \times 10^{-15}$
<i>Confining Unit, κ_c</i>	10^{-18}
Porosity:	
<i>Reservoir, ϕ_r</i>	0.10
<i>Confining Unit, ϕ_c</i>	0.10
Density [kg/m^3]:	
<i>Reservoir, ρ_r</i>	920
<i>Confining Unit, ρ_c</i>	920
Compressibility [Pa^{-1}]:	
<i>Reservoir, β_r</i>	4.5×10^{-10}
<i>Confining Unit, β_c</i>	4.5×10^{-10}
Specific Heat: [$\text{kJ}/\text{kg}\cdot\text{K}$]	
<i>Reservoir, $c_{p,r}$</i>	2.8
<i>Confining Unit, $c_{p,r}$</i>	2.8
Thermal Conductivity [$\text{W}/\text{m}\cdot\text{K}$]:	
<i>Reservoir, k_r</i>	2.0
<i>Confining Unit, k_c</i>	2.0
Reservoir Dimensions [m]	
<i>Top Depth, z</i>	2500, 3500, 5000
<i>Thickness, Δz</i>	50, 100
Temperature Gradient, G [$^\circ\text{C}/\text{km}$]	35, 50

Fluid Parameters

The heat extraction fluid in all the simulations was either water or CO_2 . Pre-existing brine or water are the conventional working fluids used in geothermal heat extraction, while CO_2 has recently been studied as a working fluid because of the added benefit of sequestration (Atrens et al., 2009; Brown, 2000; Garapati et al., 2015). The use of CO_2 as the working fluid is advantageous compared to water because of higher mobility, higher conversion efficiency in the power plant, and less pumping requirements due to density differences

between pre-existing fluid and CO₂ known as the thermosiphon effect (Adams et al., 2014). Furthermore, CO₂ is a low cost fluid that is readily available for use.

Relevant thermo-physical properties of a geo-fluid are density, specific heat capacity, thermal conductivity, and viscosity. The critical point of CO₂ is at 304.25K (31.10°C) and 7.39 MPa (1,071 psi) (Burgess, 2016). As such, CO₂ is in the supercritical phase within the reservoir (sCO₂). In the supercritical state, CO₂ has the viscosity of a gas and the density of a fluid, both of which increase with pressure (Ouyang, 2011). When comparing the two fluids, water is denser than sCO₂. Specific heat capacity is a measure of the ability of a substance to store heat, and a factor in determining the amount of energy that is extracted from a reservoir. The specific heat of water is approximately double the specific heat of sCO₂ at the conditions of the reservoir, which means water can store more heat than CO₂. Also, CO₂ has a lower viscosity than water at the conditions of the reservoir.

The fluid properties of the water that is injected into the reservoir are determined from the American Society of Mechanical Engineers (ASME) steam tables built into the NUFT code, using the pressure and temperature of the element in the mesh. The density of water at a given pressure is calculated using the linear relationship of a reference pressure and density, assuming a compressibility of $3.5 \times 10^{-10} \text{ Pa}^{-1}$, and a reference pressure and density of $1 \times 10^5 \text{ Pa}$ and $1,000 \text{ kg/m}^3$, respectively. NUFT uses the Span and Wagner (1996) tables to calculate the density and enthalpy of CO₂, and the equations in Fenghour, Wakeham, and Vesovic (1998) to calculate viscosity.

The pressure at the injection well increases as fluid is injected into the reservoir and decreases as fluid is produced from the reservoir. The change in pressure that occurs depends on fluid flow. Permeability is a measure of the ease at which fluid moves through the reservoir. A reservoir with low permeability and large mass flowrates could cause high pressure at the injection well and low pressure at the production well. As such, the injection and production mass flowrate chosen for each scenario vary by the specified permeability of the reservoir (Table 2).

Table 2: Mass Flowrate Specifications for CO₂ and water for Each Permeability; *for CO₂ only

Reservoir Permeability κ_r [m ²]:	Mass Flowrate, \dot{m} [kg/s]													
	5	10	15	20	25	40	50	75	100	150	200	250	275	300
1×10^{-11}	X	X			X		X	X	X	X	X	X		
1×10^{-12}	X	X			X		X	X	X	X	X	X	X*	X*
1×10^{-13}	X	X			X		X	X	X	X	X	X		
5×10^{-14}	X	X		X		X	X	X						
1×10^{-14}	X	X	X	X	X	X	X							
5×10^{-15}	X	X	X	X										

The mass flowrates specified for CO₂ and water are the same, but the maximum mass flowrate that is possible to simulate for a given permeability differs for water and CO₂. The high mobility of CO₂ allows for larger mass flowrates than water. For example, for the reservoir given in Figure 5 with a permeability of 1×10^{-14} m², the maximum injection

production mass flowrate possible to simulation in NUFT without inducing unrealistically high or low pressure for water is 50 kg/s and 150 kg/s for CO₂.

The surface temperature (at $z = 0$ m) was set to 15 °C, and the model was initialized for one million years so that the elements in the mesh were in thermal and hydrostatic equilibrium for the given geothermal temperature gradient, reservoir depth, and reservoir thickness prior to simulating the injection and production of fluid. The injection temperature of both water and sCO₂ was between 35 °C and 45 °C over all of the simulations conducted determined using temperature outputs from NUFT at the injection well. This injection temperature range ensures the phase of injected water is liquid and the phase of injected CO₂ is supercritical. In the input file, the enthalpy of the fluid that is injected through the injection well is specified to be 200 kJ/mole and -225 kJ/mole for water and CO₂, respectively. The NUFT model determines the temperature (T_{inj}) of this injected fluid that corresponds to the enthalpy specified for the pressure at the injection well and thermophysical properties of the fluid.

Solution Parameters

The NUFT model uses the iterative Newton-Raphson method to calculate the values of each output variable (i.e., temperature, pressure, and concentration) that is recorded for each time step. The Newton-Raphson convergence tolerance is the maximum change necessary between approximations to calculate the output variable at a given time. NUFT uses a dynamic time step to reduce computational time. This means the times at which

NUFT is calculating the magnitude of the output variables depends on the current time step. The initial time step is set to one minute, which will increase to a maximum time step of ten years as long as the absolute and relative tolerances are not reached (Table 3).

Table 3: NUFT Output Variable Tolerances

	Convergence Tolerance	Absolute Tolerance	Relative Tolerance
Temperature	0.001°C	15°C	20%
Pressure	100 Pa	1 MPa	10%
Concentration	1×10^{-3} mole fraction	0.1 mole fraction	10%

The absolute tolerance is maximum allowable change in a variable from one time step to the next, and the relative tolerance is the maximum allowable percent change in a variable from one time step to the next. The convergence tolerance, absolute tolerance, and relative tolerance for temperature, pressure, and concentration of each cell at each time step are given in Table 3. The simulation will stop running if there are more than 30,000 time steps, which ensures that the time step does not continuously decrease if a tolerance is not met. A continuously decreasing time step occurs when there is an unrealistic physical aspect in the simulation. These tolerances have been used to previous studies using NUFT.

Chapter 3: Processing Simulation Results

This chapter presents the equations used to develop the reduced form representation for temperature drawdown and energy that is extracted. Temperature of the produced fluid and energy that is extracted from all the simulations are normalized for different parameters to collapse the data onto a single curve. The Richards' curve (i.e. the generalized logistic curve) is fitted to this data to accurately predict the drawdown using the reduced form for the two working fluids, water and CO₂.

Generalized Logistic Curve

For a given combination of reservoir parameters, the temperature of the fluid being produced from the reservoir ($T_{prod,t}$) will change over time as a function of how much heat has been extracted from the reservoir through the production well (Q_t) and how much heat has been added to the reservoir from the natural geothermal heat flux (Q_{in}). The energy that is extracted at time t from the reservoir is calculated based on the enthalpy extracted from the reservoir during a period of time, Δt :

$$Q_t = \dot{m}_t \cdot c_{p,t} \cdot (T_{prod,t} - T_{inj,t}) \cdot \Delta t \quad (1)$$

Where Q_t is the energy that is extracted in a single time period [kJ], \dot{m}_t is the mass flowrate of the fluid per unit of time [kg/s], Δt that is produced from the reservoir at time t [s], $c_{p,t}$ is the specific heat of the produced fluid [kJ/kg-K], $T_{prod,t}$ is the temperature of the

produced fluid at time t [K], and $T_{inj,t}$ is the temperature of the injected fluid at time t [K]. The temperature of the injected fluid is constant for each simulation after initial fluctuation. As such, the injection temperature is assumed to be constant for the follow calculations (T_{inj}). Specific heat, c_p , changes with temperature and pressure. Since these changes are small, specific heat is assumed to be constant at the values given in Table 4 for this analysis. The value of specific heat used to calculate energy that is extracted from the reservoir is an average over a range of temperatures for isobaric conditions obtained from the NIST Webbook (Burgess, 2016). The pressure assumed for isobaric conditions is the hydrostatic pressure at the top of the reservoir (Table 4). The geothermal temperature gradient is a function of the natural heat flux (q) and the thermal conductivity of the rock (k_{rock}) given in Table 1: $q = k_{rock} G$.

Table 4: Average Specific Heat Capacity in Isobaric Conditions

Depth [m]	Hydrostatic Pressure at Top of Reservoir [MPa]	Range of Temperature [°C]	Average Specific Heat of CO ₂ [kJ/kg-K]	Average Specific Heat of Water [kJ/kg-K]
2500	24.5	35 - 140	2.11	4.16
3500	34.3	35 - 190	1.83	4.18
5000	49.0	35 - 265	1.65	4.23

In order to produce a model that is generalizable across various geologic settings and operational decisions, the results of the 300 reservoir simulations per working fluid were collapsed by fitting a generalized logistic curve to dimensionless normalizations of the temperature of the produced fluid (\bar{T}) and of the energy that is extracted from the reservoir

(\bar{Q}). This logistic curve of the form in equation 2, also known as Richards' curve (Birch, 1999; Richards, 1959), thus serves as a reduced form representation of the performance of a sedimentary basin geothermal reservoir for a range of reservoir parameters and operational decisions:

$$\bar{T} = U + \frac{L - U}{(1 + Ae^{-x(\bar{Q} - M)})^{1/\nu}} \quad (2)$$

The coefficients U , L , A , x , M , and ν are parameters of the logistic curve. The parameter U is the upper asymptote of the curve, and L is the lower asymptote of the curve, for the \bar{T} axis. The parameter M represents a shift along the \bar{Q} axis and could be considered to represent the sensitivity of the change in temperature of the produced fluid to the energy in the reservoir, whereas the parameters A , x , and ν indicate the steepness and curvature of the logistic curve and thus represent the sensitivity of the change in temperature due to the extraction of heat from the reservoir.

Data Normalization

Equation 3 is the calculation for the normalized temperature of the produced (\bar{T}). It is the difference between the temperature of the produced fluid and of the injected fluid divided by the difference between the initial temperature of the produced fluid and the temperature of the injected fluid,

$$\bar{T} = \frac{T_{prod,t} - T_{inj}}{T_{prod,t=0} - T_{inj}} \quad (3)$$

where $T_{prod,t=0}$ is the initial temperature of the reservoir [°C], $T_{prod,t}$ is the current temperature of the reservoir which is represented by the temperature of the produced fluid [°C], and T_{inj} is the average injection temperature over the entire simulation [°C]. The initial temperature of the produced fluid is a function of the depth of the top of the reservoir (z), the geothermal temperature gradient (G), and surface temperature (T_s): $T_{prod,t=0} = T_s + zG$. Since the temperature of the produced fluid at any point in time can never exceed its initial temperature or be below the injection temperature, $0 \leq \bar{T} \leq 1$. The upper asymptote of the logistic curve in equation 2, U , was set to one, because the normalization of temperature (\bar{T}) cannot be greater than one. While this normalization has a lower bound of zero, the lower asymptote, L , of the logistic curve may not be zero because there is residual heat in the reservoir between the injection well and the production well. Also, the increase in heat due to the constant background geothermal heat flux during each time step increases the temperature of the fluid between the injection well and the production well.

The cumulative amount of energy that has been extracted from the reservoir was calculated using Q_t in equation 1 for each time increment is normalized by the total amount of energy that could have been extracted from the reservoir ($Q_{tot,t}$). Since the cumulative amount of energy that is extracted from the reservoir cannot be greater than the total amount of energy that could be extracted from the reservoir, $0 \leq \bar{Q} \leq 1$.

$$\bar{Q} = \frac{\sum_{t=0}^t Q_t}{Q_{tot,t}} = \frac{\sum_{t=0}^t Q_t}{Q_{res,t=0} + \sum_{t=0}^t Q_{in,t} + \sum_{t=0}^t Q_t} \quad (4)$$

where $Q_{res,t=0}$ is the initial amount of energy that is in the reservoir at $t=0$ [kJ], and $Q_{in,t}$ is the net amount of energy that enters the reservoir due to the natural geothermal heat flux during each time step at time t [kJ]. The initial amount of energy that is in the reservoir at $t=0$ is the energy stored in the rock and naturally-present fluid,

$$Q_{res,t=0} = \pi r^2 \cdot \Delta z \cdot T_{ave,r,t=0} \cdot \left((1 - \theta_r) \cdot \rho_r \cdot c_{p,r} + \theta_r \cdot \rho_f \cdot c_{p,f} \right) \quad (5)$$

where r is the radius of the geothermal reservoir [m], Δz is the thickness of the reservoir [m], θ_r is the porosity [dim], ρ_r and ρ_f are the densities of the reservoir rock and the fluid in the pores of the reservoir, respectively [kg/m³], $c_{p,r}$ and $c_{p,f}$ are the heat capacities of the reservoir rock and the fluid in the pores of the reservoir, respectively [kJ/kg-K], and $T_{ave,r,t=0}$ is the average temperature in the reservoir at $t=0$:

$$T_{ave,t=0} = T_s + G \cdot \left(z + \frac{\Delta z}{2} \right) \quad (6)$$

where T_s is the surface temperature [K], G is the temperature gradient [K/m], Δz is the thickness of the reservoir, and z is the depth to the top of the reservoir [m].

Regeneration of Heat in the Reservoir

Heat transfer is in itself a complex process. Understanding and quantifying multiple heat transfer processes taking place simultaneously adds additional layers of complexity because of changing and often unknown properties (e.g. convective heat transfer

coefficient) over time and space. Figure 6 illustrates the different processes that take place during geothermal heat extraction, where the variable q represents a heat transfer process.

The figure assumes a geometric CO_2 plume. Specifically, these are:

- 1) q_1 = conduction through the rock of the reservoir
- 2) q_2 = convection of the water outside the CO_2 plume and the reservoir rock
- 3) q_3 = convection of CO_2 and the reservoir rock
- 4) q_4 = convection of the water to CO_2 plume
- 5) q_5 = convection of the rock surrounding the reservoir to the water inside the reservoir
- 6) q_6 = convection of CO_2 in the plume
- 7) q_7 = convection of water within and outside the reservoir

The variables above correspond to the variables in Figure 6. For the case with only water, q_3 , q_4 , and q_6 do not apply.

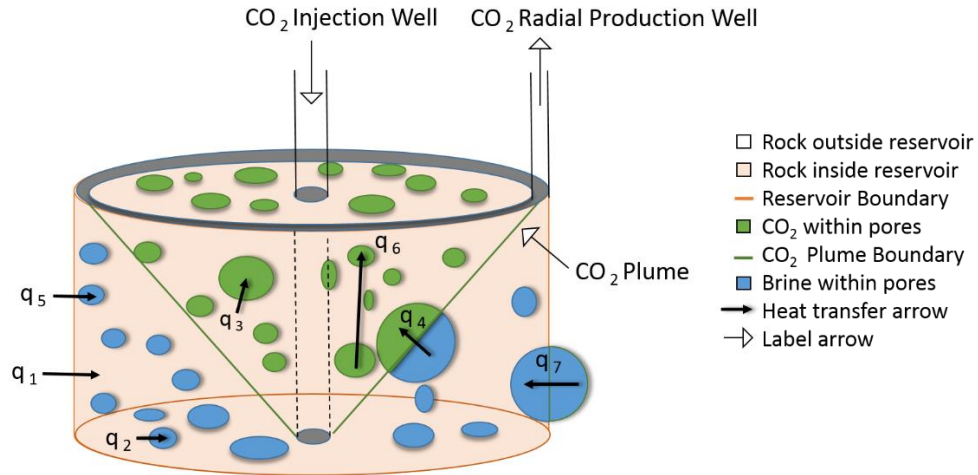


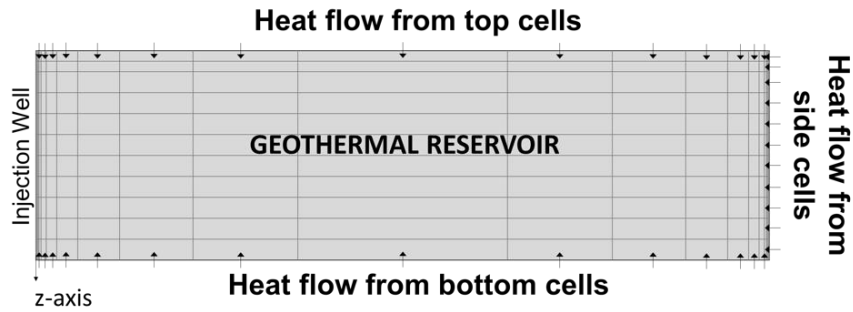
Figure 6: Reservoir Animation of a CO_2 -Plume within a Reservoir Highlighting Heat Transfer Processes

The heat that enters the reservoir depends on a variety of reservoir characteristics and operational decisions, such as the history of heat extraction and the resulting distributions of temperature and pressure in the reservoir, the physical attributes of the reservoir, and the type and size of the production system (expanded from Rybach (2007)).

There will be no net heat transfer into the reservoir from the geothermal heat flux at $t=0$ because the reservoir is in thermal equilibrium at the beginning of the simulation. The geothermal heat flux will add heat to the reservoir when the temperature in the reservoir decreases due to the injection of fluid that is colder than the reservoir ($T_{inj} < T_r$) and fluid that has been heated in the reservoir is produced from the production well. The net amount of heat that enters the reservoir at a point in time, $Q_{in,t}$, depends on the difference in temperature between each element on the inside boundary of the reservoir and the neighboring element(s) on the outside boundary of the reservoir (Figure 7(a)). When heat

is extracted from the reservoir, the temperature of the elements inside the reservoir will decrease below the state at which they are in thermal equilibrium with the surrounding rock. As such, reservoir temperature recharge from the geothermal heat flux will occur only when heat has been extracted from the reservoir. Since the temperature of the reservoir varies within the reservoir, the heat flow will vary at different areas of the reservoir, where there will be more heat flow at colder areas (i.e., the injection well). As such, NUFT outputs the net heat flow into the reservoir for each cell around the reservoir, a schematic is given in Figure 7(a). This consists of heat entering from above, below, and from the sides of the reservoir, each contributing a portion of the total heat flow into the reservoir. The sum of each cell is the total heat flow into the reservoir at a given time ($Q_{in,t}$). An example of this is shown in Figure 7(b).

(a) Schematic of Reservoir Cells



(b) Example of Heat Flow over Time

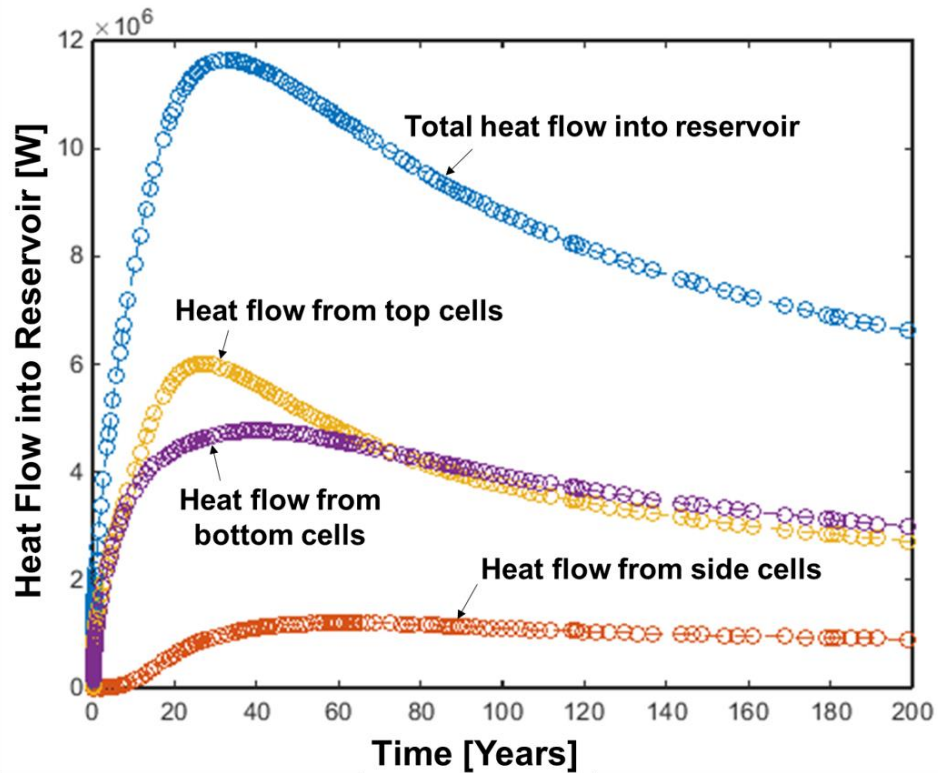


Figure 7: (a) Schematic of Reservoir Cells and (b) Example of Heat Flow into Reservoir for Simulation using Water with Parameters: Permeability(κ) = 10^{-13} m², Depth(z) = 2,500m, Temperature Gradient(G) = 50°C/km, Thickness(Δz) = 100m, Mass Flowrate(\dot{m}) = 200 kg/s

Figure 8 shows total heat flow into the reservoir over time for water and CO₂ for mass flowrates 100 kg/s and 250 kg/s. The heat flow into the reservoir for the simulations using water is larger because the temperature drawdown is greater in these scenarios. The peak of heat flow changes between scenarios, where this peak occurs later when using a smaller mass flowrate. Subsequently, the heat flow into the reservoir steadily decreases over time because the rock surrounding the reservoir has cooled. Once the heat flow into the reservoir begins to decrease, the temperature in the reservoir will take longer to recharge because a larger volume of the rock has lost heat. This cooling of the surrounding reservoir rock is an important component of the natural resource economics model because it dictates how quickly the temperature of the produced fluid decreases as energy is extracted.

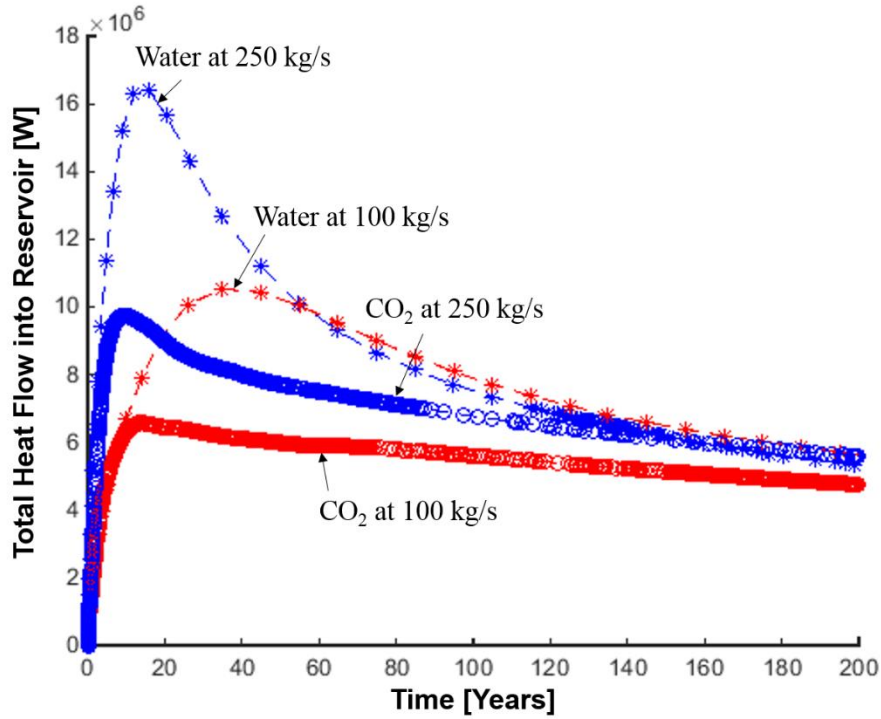


Figure 8: Heat flow into Reservoir for Water and CO₂ using a Mass Flowrate of 100 kg/s and 250 kg/s with Parameters: Permeability(κ) = 10^{-11} m², Depth(z) = 3,500m, Temperature Gradient(G) = 35°C/km, and Thickness(Δz) = 100m

The natural resource economic model that is presented in the next chapter requires a function to calculate the cumulative heat flow into the reservoir in order to determine the temperature drawdown as energy is extracted from the reservoir. As such, two parameterization analyses were performed on the data generated by NUFT to estimate the parameters in equation 8 that relate $Q_{in,t}$ to Q_t for water and CO₂ using STATA. The analysis was a maximum-likelihood estimation panel regressions in order to produce a reduced form representation of $Q_{in,t}$. The advantage of a panel regression is that it accounts for effects between multiple simulations instead of as individual data points and tends to

be a more robust analysis technique (Hu et al., 1998). The regression is of the form,

$$Q_{in,t} = \kappa^{\beta_1} \cdot z^{\beta_2} \cdot \Delta z^{\beta_3} \cdot \dot{m}^{\beta_4} \cdot G^{\beta_5} \cdot \left(\sum_{t=0}^t Q_{ex} \right)^{\beta_6} \cdot Q_{ex}^{\beta_7} \cdot t^{\beta_8} \cdot Q_{res,t=0}^{\beta_9} \quad (7)$$

where β_1 , β_2 , β_3 , β_4 , β_5 , β_6 , β_7 , β_8 , and β_9 are the parameters that were estimated by the regression. The nonlinear regression reflects the nonlinear shape of heat flow into the reservoir as seen in Figure 8. The equation is transformed as a log-linear function:

$$\ln(Q_{in,t}) = \beta_1 \ln(\kappa) + \beta_2 \ln(z) + \beta_3 \ln(\Delta z) + \beta_4 \ln(\dot{m}) + \beta_5 \ln(G) + \beta_6 \ln\left(\sum_{t=0}^t Q_{ex}\right) + \beta_7 \ln(Q_{ex}) + \beta_8 \ln(t) + \beta_9 \ln(Q_{res,t=0}) \quad (8)$$

Each term of the equation captures how the different variables, permeability, depth, thickness, mass flowrate, temperature gradient, cumulative energy that is extracted, energy that is extracted in a given time period, time, and initial energy in the reservoir, affect heat flow into the reservoir over time.

Table 5 provides the regression results to determine the net heat entering the reservoir.

Table 5: STATA Regression Results for Heat Flow into Reservoir for Water and CO₂

Working fluid:	Water	CO ₂
Regression Coefficient	Q _{in}	Q _{in}
β_1	0.0534*** (0.00458)	0.0513*** (0.0120)
β_2	-0.713*** (0.0599)	-1.093*** (0.139)
β_3	-0.510*** (0.0433)	-0.661*** (0.113)
β_4	-0.820*** (0.0174)	-1.586*** (0.0247)
β_5	-0.675*** (0.0756)	-1.687*** (0.186)
β_6	0.837*** (0.0203)	1.523*** (0.0107)
β_7	1.132*** (0.00463)	0.955*** (0.00208)
β_8	-0.0699*** (0.0167)	-0.750*** (0.00954)
β_9	-0.423*** (0.0247)	-0.111* (0.0623)
Observations	22,907	199,519
Number of Simulations	300	300

Standard errors in parentheses
 *** p<0.01, ** p<0.05, * p<0.1

Though both regressions comprise of 300 simulations each, the number of observations depends on the dynamic time step in NUFT discussed in an earlier chapter. As such, the number of observations for water scenarios (i.e. 22,907 observations) are not equal for CO₂ scenarios (i.e. 199,519 observations). All the variables in equation 7 were significant (p<0.05), except the initial energy in the reservoir for CO₂.

While permeability was significant for both water and CO₂, the effect of permeability is more drastic for CO₂ than water. Permeability affects the formation of this plume and the total time fluid spends in reservoir as seen in Figure 9.

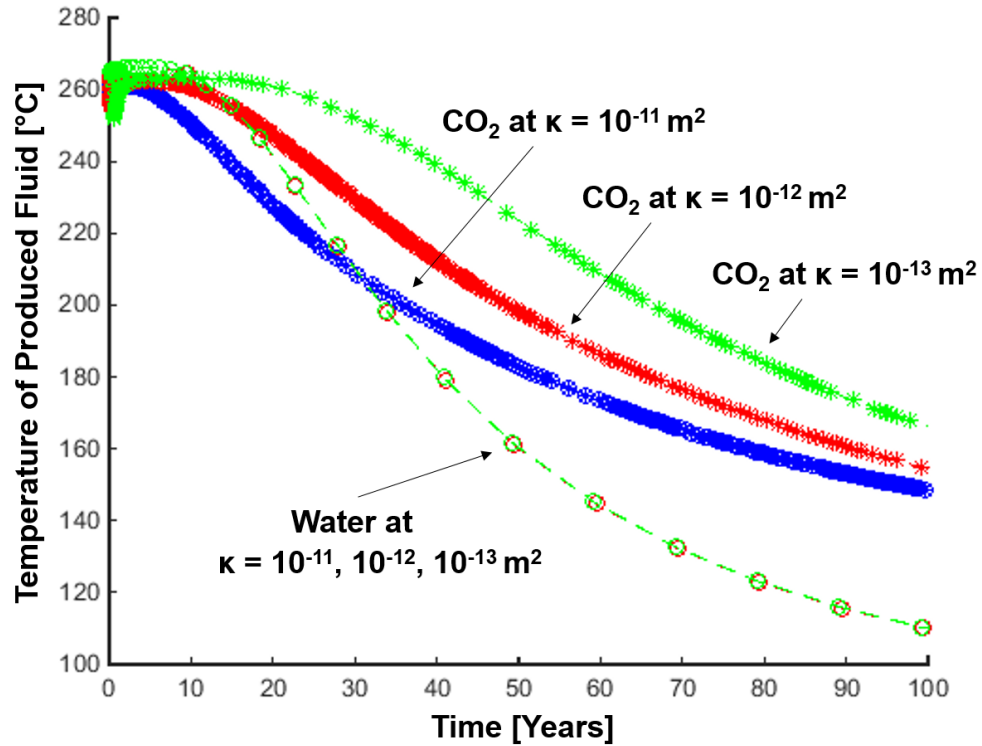


Figure 9: Change in Temperature of Produced Fluid over Time for Different Permeabilities with Parameters: Depth(z) = 5,000m, Temperature Gradient(G) = 50°C/km, Thickness(Δz) = 100m, and Mass Flowrate(\dot{m}) = 100 kg/s

According to the simulation results, different permeabilities does not affect the change in temperature of the produced water, but the temperature of produced CO₂ increases with a smaller permeability. A more permeable reservoir (e.g., 10^{-11} m^2) will form a narrower CO₂-plume, and the fluid will easily flow, decreasing the total time fluid spends in reservoir. As such, the temperature of the produced fluid quickly drops over time. On the

other hand, the scenario using CO₂ at a permeability of 10^{-13} m² maintains a higher produced fluid temperature. The results of the STATA regression for water and CO₂ were subsequently implemented into the natural resource economics model presented in the following chapter.

Chapter 4: Dynamic Optimization Model

This chapter presents the dynamic optimization model that uses a natural resource economic approach coupled with NUFT simulation results. The formulation of the model is broken down into six parts and discussed in detail: stages, state variables, decision variables, constraints, state-transition functions, and the objective-contribution function. The model uses Solver in Microsoft Excel, commonly used in dynamic programming, to solve for the optimal mass flowrate over time given a time horizon, reservoir parameters, and economic parameters.

Description of Model Objective

The goal of this model, known as the objective function, is to determine the mass flowrate over time that maximizes the net present profit of extracting heat from the reservoir and using it for economic gain:

$$\max \Xi = \sum_{s=1}^s \frac{\xi \cdot Q_s}{(1 + \delta)^{\tau_s}} \quad (9)$$

where Ξ is the present value of net profit over the time horizon [\$], δ is the discount rate [%] and ξ is net profit per unit of energy that is extracted from the reservoir [\$/kJ]:

$$\xi = \eta_w \cdot \eta_p \cdot (p - c_t) \quad (10)$$

where η_w is a factor that represents the efficiency by which the energy of the fluid that is produced from the reservoir is maintained through the production well [dim], η_p is the efficiency of the power plant that converts heat into electricity [dim], p is the selling price of energy [\$/kJ], and c is the levelized cost of energy (LCOE) as a function of energy that is extracted [\$/kJ]:

$$c_t = \frac{C_{t=0}}{(\dot{m} \cdot c_p \cdot T_{prod,t} \cdot \Delta\tau)} \quad (11)$$

where $C_{t=0}$ is the initial investment cost [\$/]. As the amount of energy that is extracted decreases due to, for example, temperature drawdown in the reservoir, the LCOE increases. The investment cost of geothermal energy depends on power plant type (e.g., binary or dry steam), resource type (e.g., sedimentary basin or EGS), drilling costs, and number of wells. The cost of geothermal power can vary depending on operation and maintenance cost, resource characteristics (e.g., depth and temperature gradient), and well productivity (Sanyal, 2004). The efficiencies are hereafter represented by a single efficiency factor (η). Furthermore, the natural resource economics model assumes a constant efficiency, selling price of electricity, and investment cost. The function Ξ in equation 9, the present value of net benefits of energy that is extracted [\$/], is the state of the system that the dynamic program in the following section seeks to maximize. This function is subject to changes over time as decisions are made because of changes in the temperature of the produced fluid as energy is extracted.

Decision and State Variables

The optimization problem uses equal time steps, $\Delta\tau$, in contrast to the dynamic time step in the NUFT model, Δt . A decision period is the length of time over which a decision is made. The duration of which is:

$$\Delta\tau = \frac{\Omega}{\omega} \quad (12)$$

where Ω is the planning horizon [years] and ω is the total number of decisions that will be made [dim]. A decision variable is controlled and decided by an operator. In the following optimization model, the decision variable is the mass flowrate of the injected and produced fluids, which are assumed to be equal for the same reasons they were equalized in the NUFT simulations (see Chapter 2). This decision variable is bounded by a lower and upper bound of the mass flowrate, which depends on the reservoir characteristics:

$$\underline{\dot{m}_f} \leq \dot{m}_f \leq \overline{\dot{m}_f} \quad (13)$$

The objective function depends on state variables. The state of a system changes as decisions are made. There is a single state in this system: the temperature of the produced fluid at any given time. Temperatures used within the model are in Kelvin to ensure that all states are positive.

The state-transition function describes how the state of a system changes as decisions are made, where s denotes the current decision period. The state transition function in this

model uses the logistic function presented in equation 4 to determine the temperature of the produced fluid as energy is extracted:

$$T_{prod,s} = \left[1 + \frac{L-1}{(1+Ae^{-x(\bar{Q}_s-M)})^{1/v}} \right] (T_{prod,\tau=0} - T_{inj}) + T_{inj} \quad (14)$$

where \bar{Q}_s is the normalized energy that is extracted using:

$$\bar{Q}_s = \frac{Q_s}{Q_{tot,s}} = \frac{Q_s}{Q_{res,s=1} + \sum_{s=1}^s Q_{in,t} + Q_s} \quad (15)$$

where

$$Q_s = Q_{s-1} + \dot{m}_{f,\Delta\tau} \cdot c_p \cdot (T_{prod,s-1} - T_{inj}) \cdot \Delta\tau \quad (16)$$

The natural resource economic model assumes that in the case with CO₂ injection and production, the CO₂ plume has already formed and the fluid being produced from the production well is CO₂. As such, the initial energy in the reservoir for water is:

$$Q_{res,s=1} = \pi r^2 \cdot \Delta z \cdot (T_{ave,r,s=1} - T_{inj}) \cdot ((1-\theta) \cdot \rho_r \cdot c_{p,r} + \theta \cdot \rho_f \cdot c_{p,f}) \quad (17)$$

and, for CO₂:

$$Q_{res,s=1} = \left(\frac{1}{3}\right) \cdot \pi r^2 \cdot \Delta z \cdot (T_{ave,r,s=1} - T_{inj}) \cdot ((1-\theta) \cdot \rho_r \cdot c_{p,r} + \theta \cdot \rho_{CO_2} \cdot c_{p,CO_2}) \quad (18)$$

where r is the distance between the wells [m], Δz is the thickness of the reservoir [m], ρ is the density [m³], c_p is the specific heat [kJ/kg-K], and θ is the porosity.

Input, Output, and Fixed Parameters

The injection temperature of the working fluid (T_{inj}) is assumed to be constant over time at 35°C to ensure CO₂ is in the supercritical phase within the reservoir. The model assumes the rock properties of the reservoir to be 920 kg/m³, 2.8 kJ/kg-C, and 2.0 W/m-C for density, specific heat, and thermal conductivity, respectively. From these inputs, the model determines specific heat of the fluid at the given depth (see Table 4). The porosity and well distance is fixed at 0.1 and 700m. These are the same parameters used in the NUFT simulations.

The user input variables of the model are presented in Table 6. The density and specific heat are given in Table 4. The output variables are given in Table 7.

Table 6: Input Parameters of Natural Resource Economic Model

Input Parameter	Unit
Planning Horizon, Ω	Years
Total Number of Stages, ω	-
Extraction Fluid, f	-
Reservoir Depth, z	m
Reservoir Thickness, Δz	m
Permeability, κ	m^2
Temperature Gradient, G	K/km
Temperature of Injection Fluid, T_{inj}	K
Mass Flowrate Boundaries, \dot{m}	kg/s
Selling Price of Energy, p	\$/kJ
Investment Cost, $C_{t=0}$	\$
Discount Rate, δ	%
Power Plant and Wellbore Efficiency, η	%

Table 7: Output Parameters of Optimal Path

Output Parameter	Unit
Mass flowrate, $\dot{m}_{f,s}$	kg/s
Temperature of Produced Fluid, $T_{prod,s}$	K
Present Value of Net Profit, Ξ_s	\$

Solution Method

The natural resource economic model was set-up in Microsoft Excel and solved using the Solver add-in. The program was set to use Generalized Reduced Gradient (GRG) Nonlinear as the solving method since the objective function is nonlinear. It requires three specifications: objective cell, decision cell(s), and constraint(s). The program requires initial guesses be set for the decision variables, known as seeding, and adjusts them to maximize the objective and to satisfy the limits on any constraints set. The program returns a solution if one is found or returns that the problem is infeasible, meaning that there is no possible solution to the given problem. While this is a great problem for smaller problems, the program is limited in terms of how many decision variables a problem can have. Moreover, there have been known issues with solutions being biased to the initial guess since the initial guess is a departure point for the solution. Though seeding is not always an issue, it is necessary to be aware of it when analyzing solution results.

Chapter 5: Results

This chapter presents results for NUFT simulations using water and CO₂, the regression analysis of the heat flow into the reservoir (Q_{in}) data for water and CO₂, and the optimal decision path over time using the dynamic optimization model.

Geothermal Reservoir Performance

Geothermal reservoir performance depends on the temperature of the produced fluid, which is a function of the amount of heat that is extracted from the reservoir. Figure 10 shows an example of the results from a NUFT simulation using water as the working fluid for a reservoir with one of the combinations of reservoir parameters studied. Figure 10(a) shows the change in temperature of produced fluid over time for three mass flowrates: 25 kg/s, 100 kg/s, and 200 kg/s. The temperature of the produced fluid decreases over time as cool fluid is injected into, and warm fluid is produced from, the reservoir. For any mass flowrate, the temperature of the produced fluid will decrease over time until the energy that is extracted from the reservoir by that produced fluid equals the energy that is added to the reservoir by the natural geothermal heat flux. Holding everything else constant, a higher mass flowrate will extract more energy than a lower mass flowrate, so that the temperature of the produced fluid decreases more and earlier in time for higher mass flowrates. This effect is shown in Figure 10(a), which also shows that the decrease in the temperature of

the produced fluid reaches an asymptote, and the temperature of the produced fluid is relatively constant over time for the scenarios with a mass flowrate of 100 kg/s and 200 kg/s. While the scenario with 25 kg/s seems that will also reach an asymptote, it has not in the figure.

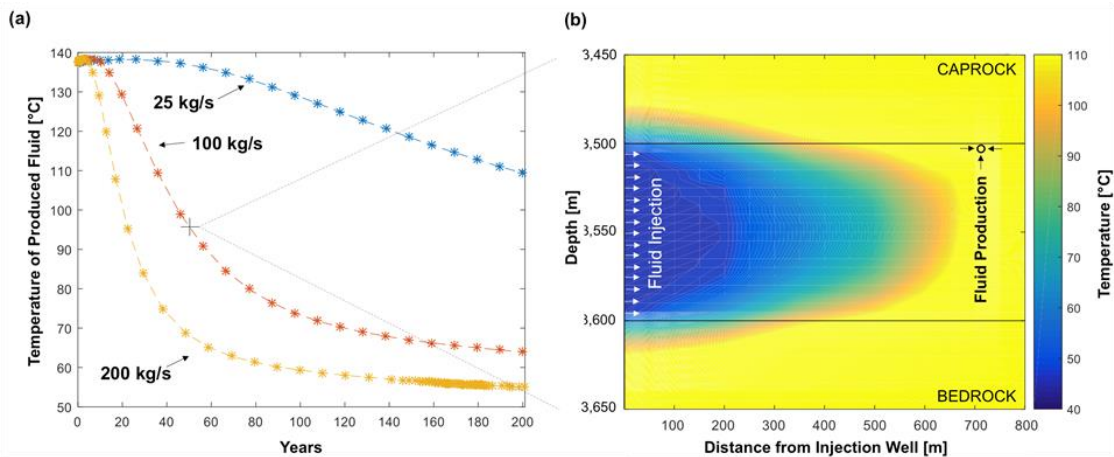


Figure 10: Example Reservoir Simulations Results Using Water from NUFT with Parameters: Permeability(κ) = 10^{-11} m², Depth(z) = 3,500m, Temperature Gradient(G) = 35°C/km, Thickness(Δz) = 100m, and (a) Varying Mass Flowrate and (b) Mass Flowrate(\dot{m}) = 100 kg/s

The asymptote will be lower for higher mass flowrates because more energy is being extracted from the reservoir. Figure 10(b) shows the temperature distribution of a cross section of the subsurface, including the sedimentary geothermal reservoir, after 50 years of continuous fluid injection and continuous fluid production for a mass flowrate of 100 kg/s. The coldest portion of the reservoir is clearly next to the injection well, where fluid is being injected into a reservoir that is hotter than the injected fluid, and the temperature profile from cool to warm in the reservoir extends laterally and slightly upward toward the

production well, where energy is being extracted from the reservoir. The initial temperature of the produced fluid in this scenario was 137.5°C, but continuous heat extraction from the reservoir has cooled off the surrounding temperature to at most 110°C.

CO₂ Fluid Production

In the scenarios using CO₂ as the working fluid, the fluid being produced from the production well is water that is naturally present within the reservoir. Breakthrough is the term given to the point in time when injected CO₂ reaches the production well. This time varies depending on mass flowrate and other reservoir conditions, ranging from one month to five years (Figure 11). The sensitivity of breakthrough time depending on mass flowrate is larger with smaller flowrates and the breakthrough time is more similar for large mass flowrates. Figure 11 shows the time of breakthrough, defined as when the mole fraction of CO₂ reaches 0.09.

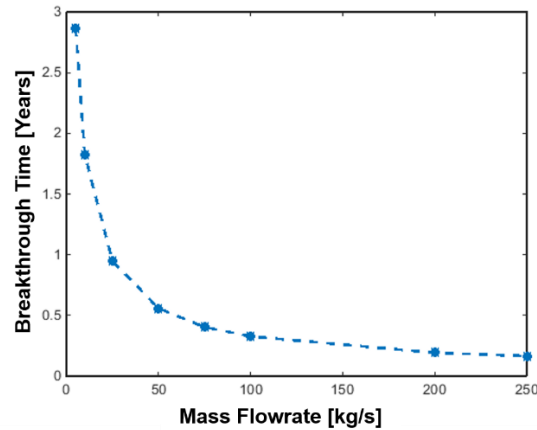


Figure 11: Breakthrough Time for Varying Mass Flowrates with Parameters: Permeability(κ) = 10^{-13} m², Depth(z) = 2,500m, Temperature Gradient(G) = 35°C/km, Thickness(Δz) = 100m, and Average Mole Fraction of CO₂ in the Production Well at Breakthrough Time: 0.09

After some time, CO₂ production from the production well reaches approximately 97-99% with the remaining fluid being residual water. The residual water is an effect of CO₂ solubility that depends on a variety of conditions including temperature and pressure (Pistone and Horne, 2011). Residual water in the production fluid will change the thermo-physical properties of the fluid, such as specific heat capacity and thermal conductivity. A scenario with a permeability of 10^{-11} m² and mass flowrate of 100 kg/s has a mole fraction of 99% CO₂ in the production well at ~32 days. A second scenario with a permeability of 5×10^{-15} m² and a mass flowrate of 20 kg/s has a mole fraction of 99% CO₂ at ~1762 days (~4.83 years). Figure 12 shows an example of the change in the temperature of the produced fluid over time and a cross section of the CO₂ plume as breakthrough and CO₂ production occur. The temperature of the produced fluid drops when breakthrough occurs

and steadily increases. This effect is due to the high buoyancy of CO₂ that causes the fluid to rush to the top of reservoir and sweep heat from the top of the reservoir where the temperature is cooler compared to the bottom of the reservoir. As more fluid is injected and the plume widens, the CO₂ sweeps heat from lower parts of the reservoir where the temperature is higher (Buscheck et al., 2016).

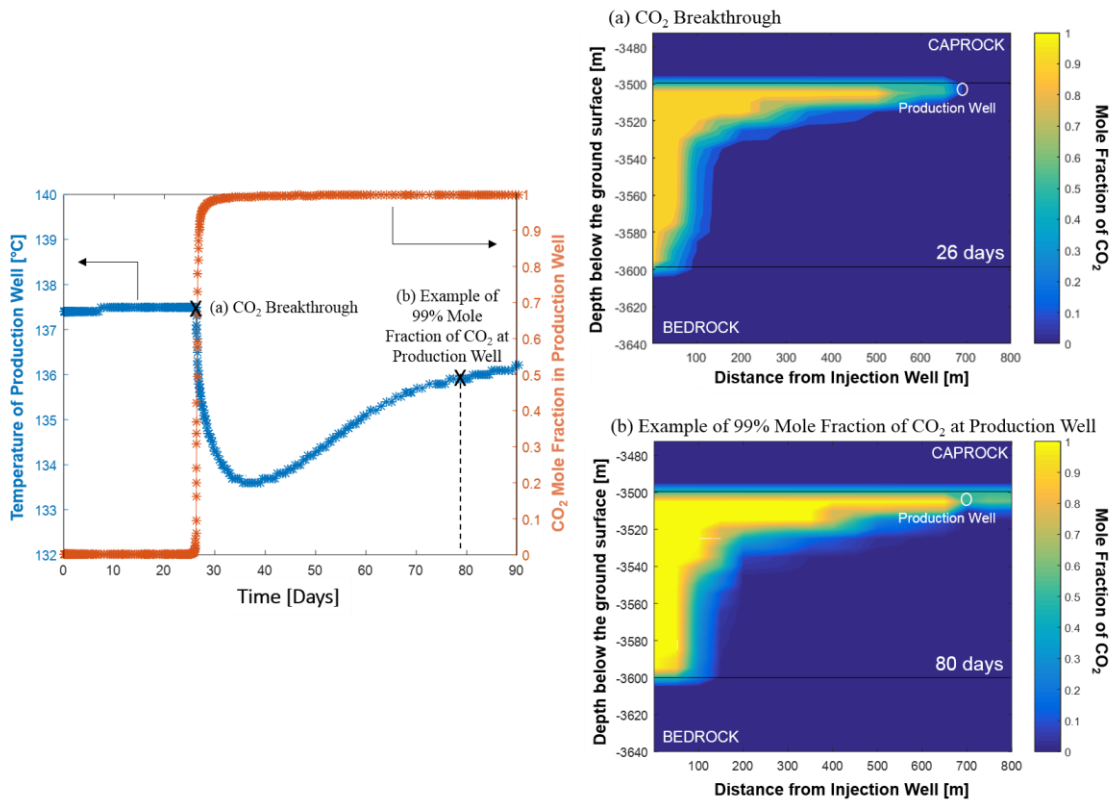


Figure 12: Example of (a) CO₂ Breakthrough and (b) 99% Mole Fraction of CO₂ at Production Well with Parameters: Permeability(κ) = 10^{-11} m², Depth(z) = 3,500m, Temperature Gradient(G) = 35°C/km, Thickness(Δz) = 100m, and Mass Flowrate(\dot{m}) = 100 kg/s

Comparing Temperature Drawdown of Water and CO₂

While the temperature of the produced fluid is central to the magnitude of heat a power plant can extract, this temperature reflects the temperature distribution within the reservoir itself.

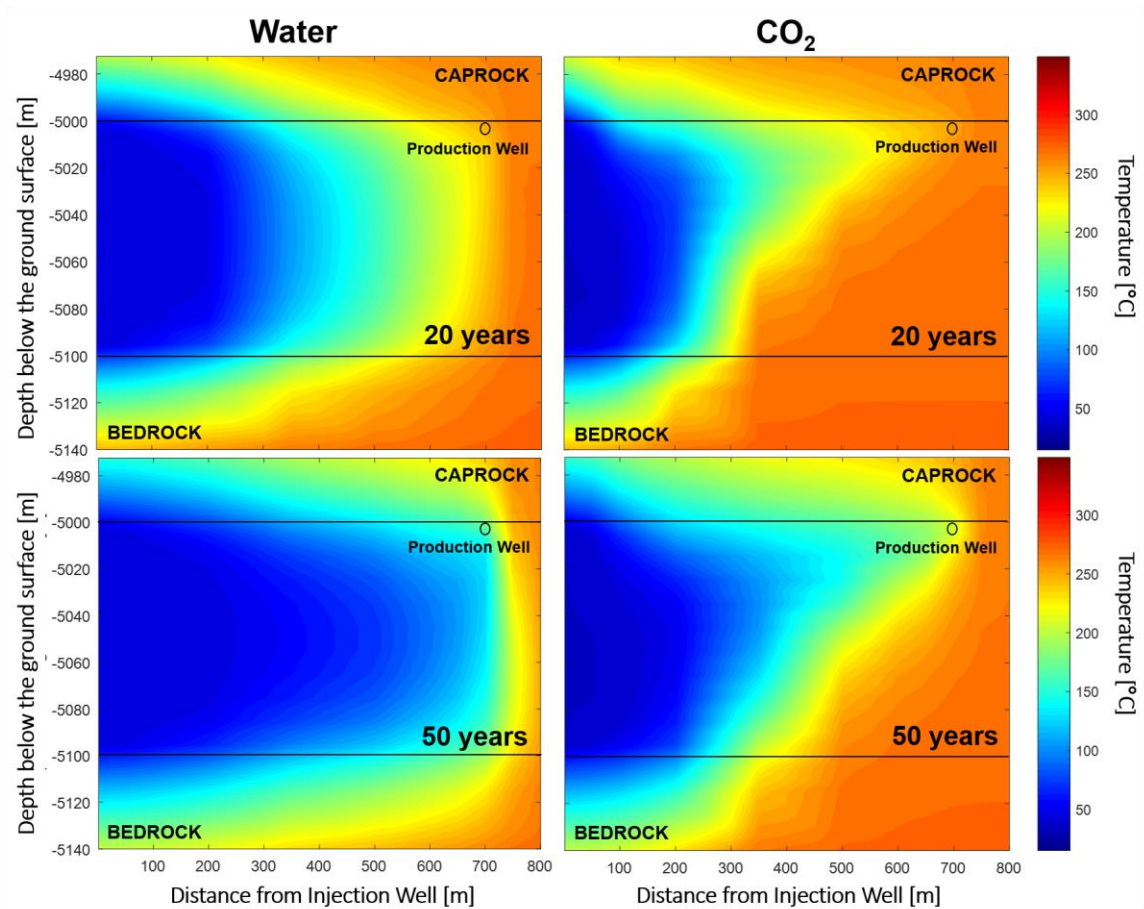


Figure 13: Temperature Drawdown in the Reservoir Using Water and CO₂ with Parameters: Permeability(κ) = 10^{-12} m², Depth(z) = 5,000m, Temperature Gradient(G) = 50°C/km, Thickness(Δz) = 100m, and Mass Flowrate(\dot{m}) = 100 kg/s

As the reservoir cools down, the temperature of the produced fluid decreases, and the time it would take to restore the reservoir to its original temperature increases. The temperature

distribution within a reservoir varies for the two extraction fluids used as seen in Figure 13 at 20 and 50 years. As seen in Table 4, water has approximately double the specific heat capacity of CO₂, where the average specific heat is 1.86 kg/km-C and 4.19 kg/km-C for water and CO₂, respectively. This means it takes approximately twice the amount of energy to raise one gram of water by 1°C compared to sCO₂. The magnitude of the specific heat explains why a larger portion of the reservoir cools down when using water. Nonetheless, CO₂ has a larger mobility compared to water so larger mass flowrates can be used with CO₂ than with water, allowing more heat to be extracted (Adams et al., 2014). This increase in mass flowrate of CO₂ offsets the smaller specific heat associated with CO₂.

Normalization Results

The temperature data that were generated in every NUFT simulation were used to determine \bar{T} and \bar{Q} . Figure 14 and Figure 15 shows these data for individual depths and all data on a single curve. A MATLAB code was written to estimate the parameters that fit the generalized logistic curve in equation 2 to the normalized data, which is shown in red. This code is given in the appendix.

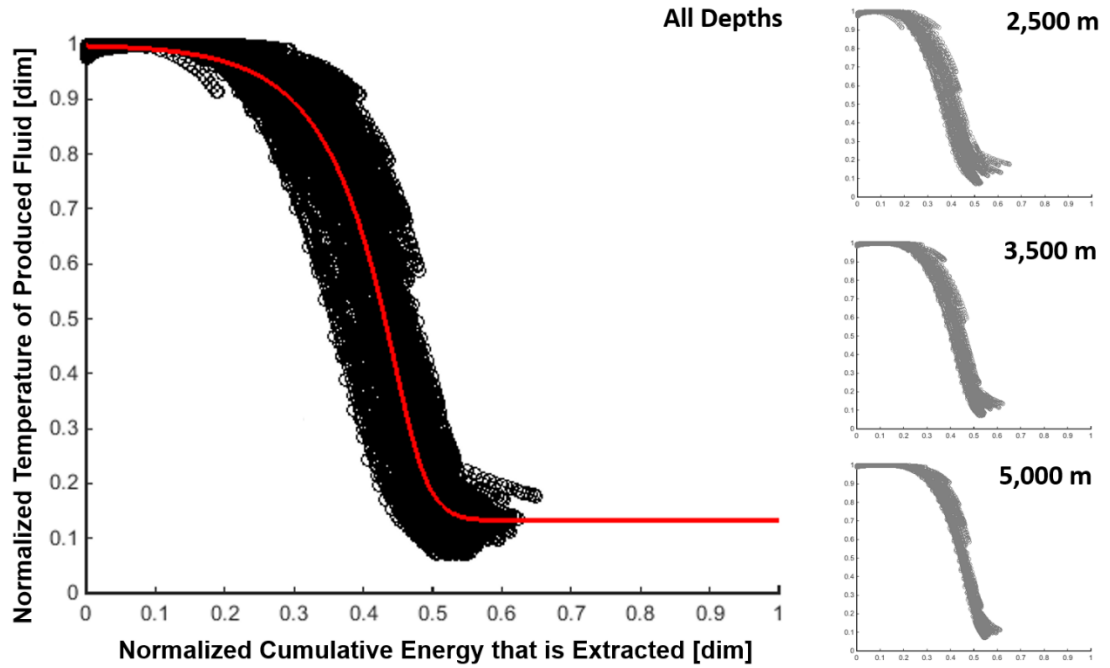


Figure 14: Normalization of the Temperature of the Production Fluid as a Function of the Energy that is Extracted from the Reservoir for NUFT Simulations Using Water

Table 8 shows the logistic curve coefficients estimated for curve fit in Figure 14.

Table 8: Coefficients of the Logistic Curve Fit to the Normalized Temperature and Heat Extraction Data Using Water

Coefficient	2,500 m	3,500 m	5,000 m	All Depths
L	0.1315	0.1220	0.1160	0.1318
A	22.31	47.07	38.35	42.46
x	38.78	82.25	63.53	49.50
M	0.3642	0.4420	0.4481	0.3986
v	3.262	7.252	4.931	4.100
r^2	0.98109	0.99033	0.99421	0.97931
Standard Error	0.0458	0.0371	0.0283	0.0564

The state-transition function in the dynamic program for water thus becomes:

$$T_{prod,s} = \left[1 - \frac{0.8682}{1 + 42.46 \cdot e^{-49.50(Q_s - 0.3986)^{1/4.1}}} \right] \bullet (T_{prod,\tau=0} - T_{inj}) + T_{inj} \quad (19)$$

The normalized data for water has a smaller spread with increasing depth. The normalized data for each depth trace out the same general trend, regardless of the depth of the reservoir, but the width of the envelope in which these normalized data fall decreases as the depth of the reservoir increases.

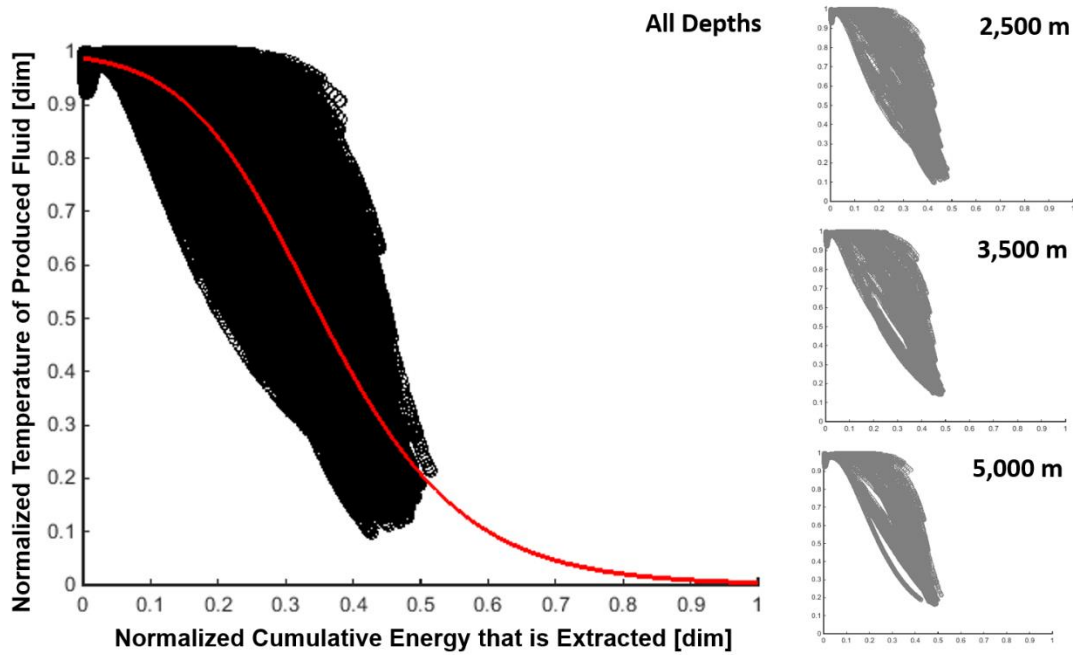


Figure 15: Normalization of the Temperature of the Production Fluid as a Function of the Energy that is Extracted from the Reservoir for NUFT Simulations Using CO₂

Table 9 shows the logistic curve coefficients estimated for the curve fit in Figure 15.

Table 9: Coefficients of the Logistic Curve Fit to the Normalized Temperature and Heat Extraction Data Using CO₂

Coefficient	2,500 m	3,500 m	5,000 m	All Depths
L	7.0562e-9	5.4652e-8	3.3253e-8	4.2653e-7
A	2.6265	0.31339	0.8728	0.32039
x	8.506	8.4286	9.2164	8.2254
M	0.12378	0.37542	0.33208	0.97957
v	0.48782	0.48645	0.69899	0.48049
r ²	0.91327	0.92271	0.93229	0.92311
Standard Error	0.0806	0.0842	0.0800	0.0831

The state-transition function in the dynamic program for CO₂ thus becomes:

$$T_{prod,s} = \left[1 + \frac{1 - (4.2653e-7)}{1 + 0.32039 \cdot e^{-8.2254(Q_s - 0.97957)^{0.48049}}} \right] \bullet (T_{prod,\tau=0} - T_{inj}) + T_{inj} \quad (20)$$

The logistic fit is better for results using water than CO₂, in part due to permeability. The following figures (Figure 16 and Figure 17) further explore the reason for the large width of Figure 15. Figure 16 parts the simulations by three permeabilities, 1x10⁻¹¹ m², 1x10⁻¹² m², and 1x10⁻¹³ m², and plots the normalization of the temperature of the produced fluid as a function of the energy that is extracted from the reservoir.

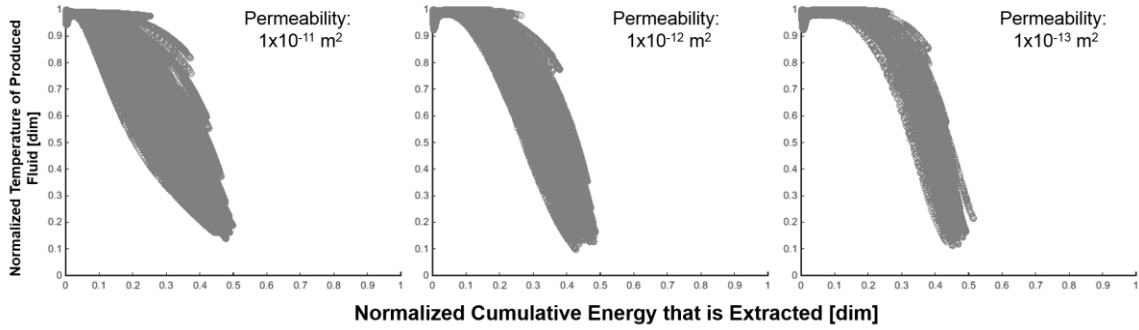


Figure 16: Normalization of the Temperature of the Production Fluid as a Function of the Energy that is Extracted from the Reservoir for NUFT Simulations Using CO₂ Parted by Permeability (κ): $1 \times 10^{-11} \text{ m}^2$ (79 Simulations), $1 \times 10^{-12} \text{ m}^2$ (77 Simulations), $1 \times 10^{-13} \text{ m}^2$ (72 Simulations)

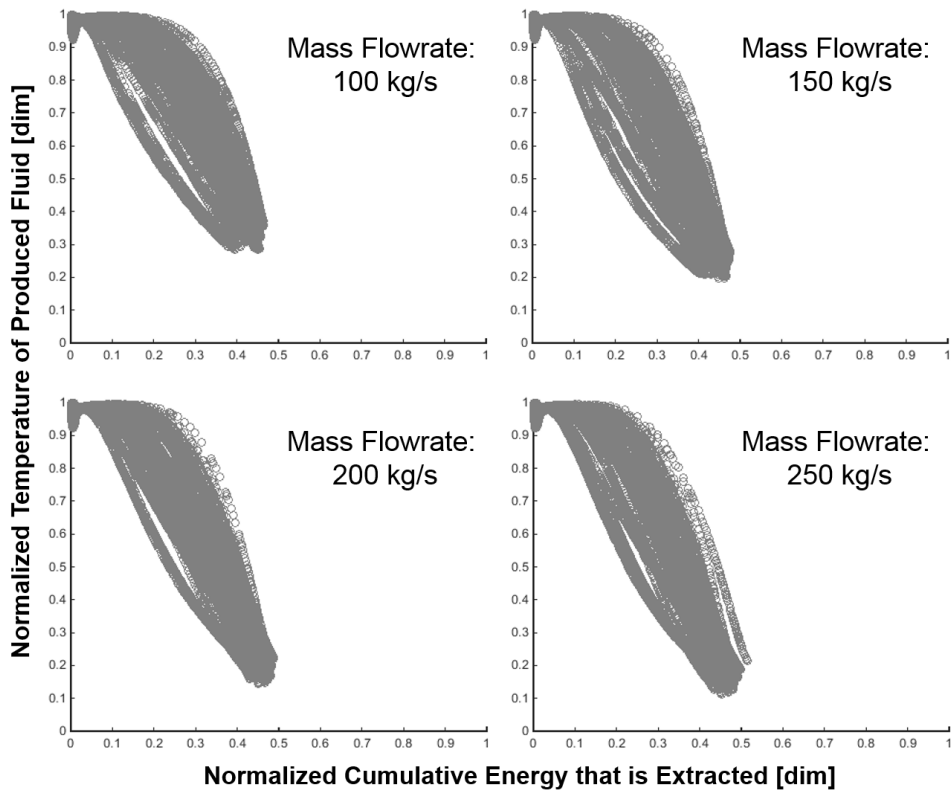


Figure 17: Normalization of the Temperature of the Production Fluid as a Function of the Energy that is Extracted from the Reservoir for NUFT Simulations Using CO₂ Parted by Mass Flowrate (\dot{m}): 100 kg/s (39 Simulations), 150 kg/s (34 Simulations), 200 kg/s (34 Simulations), 250 kg/s (33 Simulations)

Figure 17 separates the simulations by four mass flowrates, 100 kg/s, 150 kg/s, 200 kg/s, and 250 kg/s, and plots the normalization of the temperature of the produced fluid as a function of the energy that is extracted from the reservoir. While the mass flowrate does not change the spread of the data, the temperature drawdown of the production fluid increases with mass flowrate. It is worthwhile to further investigate the spread of Figure 15 to better collapse the data onto a single curve, specifically understanding the role permeability plays in how temperature of the produced fluid changes.

When using water the as working fluid, it is expected that the production temperature will be constant initially, but then will quickly decrease until it reaches a temperature close to, but not exactly, the injection temperature. In the case of CO₂, the temperature of the produced fluid gradually decreases as energy is extracted. Because water extracts more energy due to its large specific heat than CO₂ at the same mass flowrate, movement along the x-axis is faster for water than movement along the x-axis for CO₂. Another noticeable difference between the normalizations is the lower asymptote. The lower asymptote of normalized temperature of produced water, U , is 0.1318, while the lower asymptote of normalized temperature of produced CO₂ approaches zero. This indicates that when using water as the working fluid, the lowest temperature of the produced fluid will approximately 13% larger than the injection temperature. The constant heat flux moving through the earth regenerates enough heat to maintain the reservoir at that temperature. On the other hand, using CO₂ reaches production temperatures much closer to the injection temperature.

Comparison of Normalization Results using NUFT Data and STATA Regression

While the figures above use raw NUFT Data for the heat flow into the reservoir, the natural resource economic model will use the previously presented STATA regression to calculate heat flow into the reservoir. The following equations are the results of the regression for water (equation 17) and CO₂ (equation 18).

$$Q_{in,t} = \frac{\kappa^{0.0534} \cdot \left(\sum_{t=0}^t Q_{ex} \right)^{0.837} \cdot Q_{ex}^{1.132}}{z^{0.713} \cdot \Delta z^{0.510} \cdot \dot{m}^{0.820} \cdot G^{0.675} \cdot t^{0.0699} \cdot Q_{res,t=0}^{0.423}} \quad (21)$$

$$Q_{in,t} = \frac{\kappa^{0.0513} \cdot \left(\sum_{t=0}^t Q_{ex} \right)^{1.523} \cdot Q_{ex}^{0.955}}{z^{1.093} \cdot \Delta z^{0.661} \cdot \dot{m}^{1.586} \cdot G^{0.1687} \cdot t^{0.750} \cdot Q_{res,t=0}^{0.111}} \quad (22)$$

In order to study the implications of the reduced-form representation, the equations were applied to the normalization and plotted (Figure 18). The overall trend of the data is captured, but there are abnormalities seen towards the end of certain simulations in the form of backward curvature. These abnormalities are seen more distinctly in the water scenario. It takes place in the simulations with smaller mass flowrates. The reason for this curvature is that the STATA regression over calculate the heat flow into the reservoir for cases with small mass flowrates after a large portion of heat has been extracted. While it is worthy to further explore this in order to more accurately parameterize heat flow into the reservoir for extreme cases, this regression is sufficient for the scenarios that will be explored though the natural resource economic model. In other words, the simulations capture 200 years of heat flow, while the natural resource economics model will simulate much smaller time horizons.

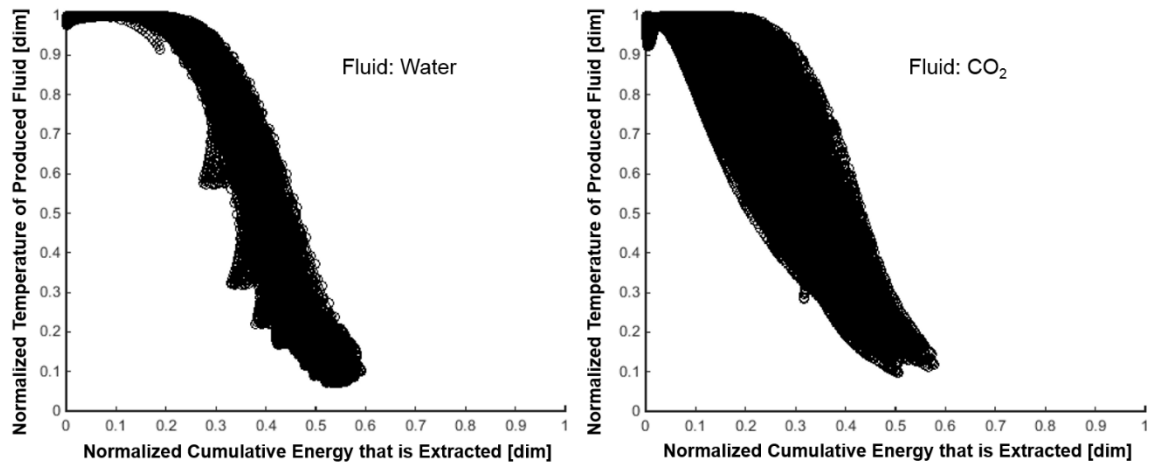


Figure 18: Normalization of the Temperature of the Production Fluid (Water and CO₂) as a Function of the Energy that is Extracted from the Reservoir for NUFT Simulations Using STATA Regression

Optimal Operation of a Geothermal Reservoir

The results of the fitted generalized logistic curve and the STATA regression on cumulative net heat into the reservoir are parts for the natural resource economic model. The following optimization results of the natural resource economics model use the parameters provided in Table 10 unless specified otherwise. The investment cost used for these results is taken from an estimation by Stefánsson (2002) for two wells and a 20MW power plant. This estimation is for a specific geothermal field and power plant parameters and will change depending on the given power plant and resource type. But, since the investment cost is not the focus of this study, this value is taken as an assumption for the investment cost in this model.

Table 10: Input Parameters Used for Following Results Unless Specified Otherwise

Input Variable	Value
Planning Horizon, Ω	50 years
Total Number of Stages, ω	50
Mass Flowrate Boundaries, Water	$0 \leq \dot{m} \leq 250$ kg/s
Mass Flowrate Boundaries, CO ₂	$0 \leq \dot{m} \leq 350$ kg/s
Fluid Injection Temperature, T_{inj}	308.15 K (35°C)
Selling Price of Energy, p	$\$2.78e-6$ /kJ
Investment Cost, $C_{t=0}$	$\$2,500,000$
Power Plant and Wellbore Efficiency, η	0.1
Discount rate, δ	5%

For scenarios using water and CO₂, Figure 19 and Figure 21, respectively, show the optimal mass flowrate over time determined by the natural resource economic model for the given parameters. The maximum mass flowrate for CO₂ is set higher than the maximum mass flowrate for water because of differences in viscosity. For both fluid scenarios, it is optimal to extract energy at the maximum mass flowrate for the entire time horizon. For water, the temperature of the produced fluid and, in turn, the net benefits decrease over time (Figure 20). Still, the decrease in the temperature can be compensated for by a large mass flowrate. On the other hand, the CO₂ scenario has little to no temperature drawdown over the time horizon, and the temperature begins to increase after approximately 25 years. The temperature drawdown of CO₂ is not being captured adequately by the natural resource economics model and the results shown have a high level of uncertainty. It will be important to investigate the cause of this to reduce uncertainty in the results of the model. The cost multiplier is a function of mass flowrate, temperature of produced fluid, and the

specific heat. It shows how the cost of electricity will increase as the temperature of the produced fluid increases. This is the economic tradeoff being made in the model.

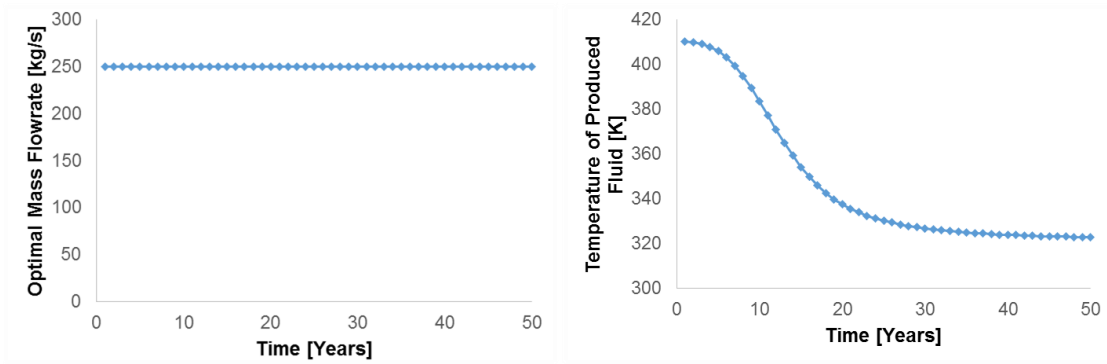


Figure 19: Optimal Mass Flowrate Time Path for Water using the Natural Resource Economics Model with Parameters: Permeability (κ) = 10^{-13} m², Depth (z) = 3,500m, Temperature Gradient (G) = 35°C/km, and Thickness (Δz) = 100m

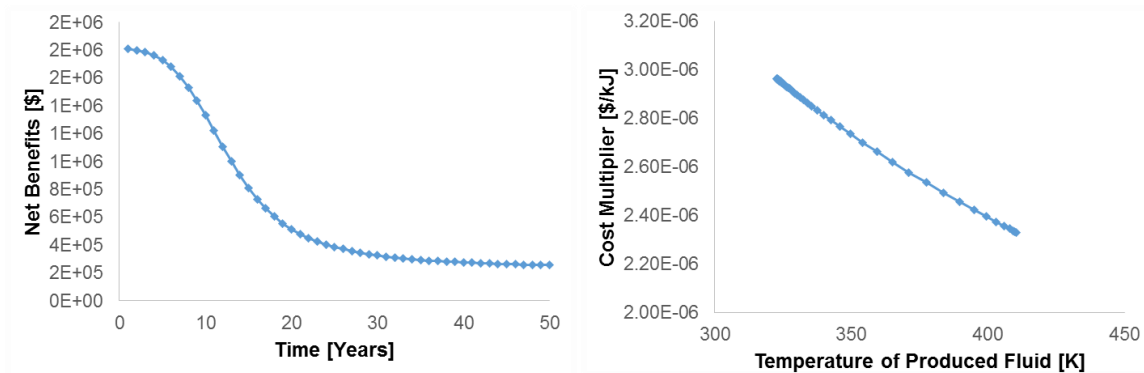


Figure 20: Economic Benefits and Cost Multiplier for Water using the Natural Resource Economics Model with Parameters: Permeability (κ) = 10^{-13} m², Depth (z) = 3,500m, Temperature Gradient (G) = 35°C/km, and Thickness (Δz) = 100m

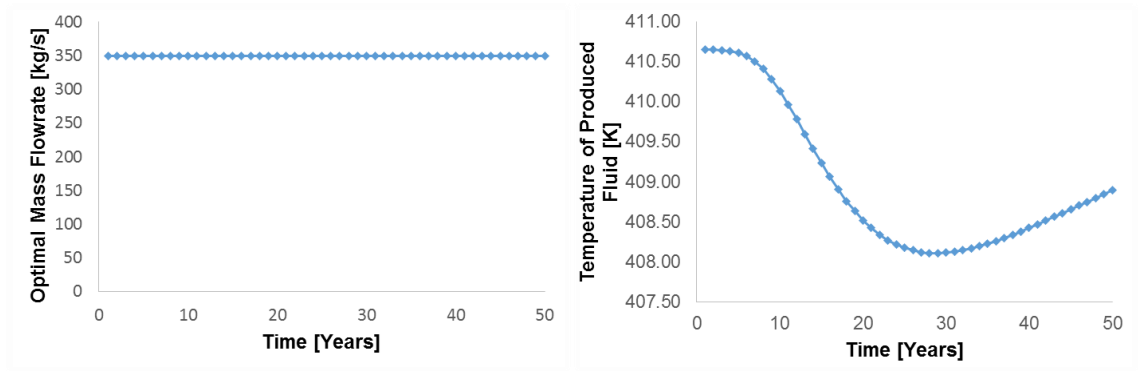


Figure 21: Optimal Mass Flowrate Time Path for CO₂ using the Natural Resource Economics Model with Parameters: Permeability (κ) = 10^{-13} m², Depth (z) = 3,500m, Temperature Gradient (G) = 35°C/km, and Thickness (Δz) = 100m

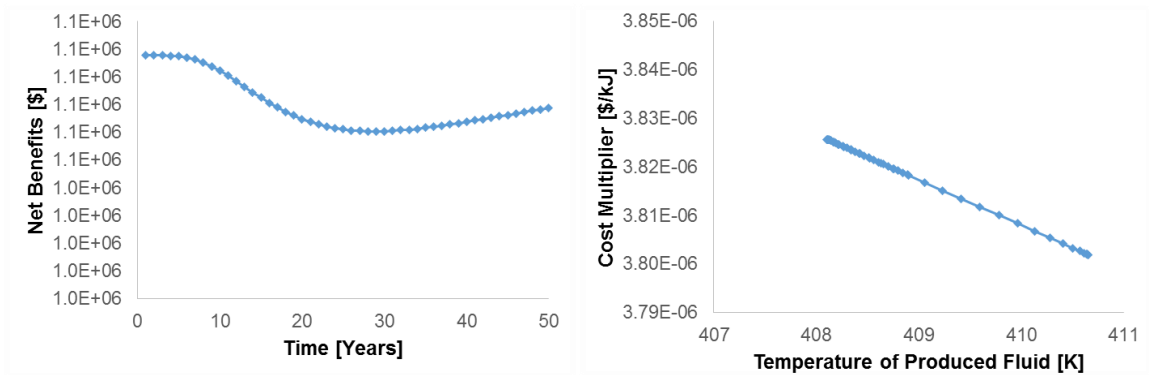


Figure 22: Economic Benefits and Cost Multiplier for CO₂ using the Natural Resource Economics Model with Parameters: Permeability (κ) = 10^{-13} m², Depth (z) = 3,500m, Temperature Gradient (G) = 35°C/km, and Thickness (Δz) = 100m

The optimal mass flowrate time path result shown in the previous figures is the result for varying reservoir depths, thickness, permeability, and temperature gradient. This implies that the model is not sensitive to the temperature drawdown of the reservoir. While there is a loss in net benefits, a large mass flowrate can compensate for this. The cost equation used in the current model is an assumption of how the LCOE changes with the amount of energy that is extracted. With a different type of assumption, i.e., a different cost function, the result of the natural resource economics will change accordingly.

Chapter 6: Future Research and Conclusion

The implications of these results are discussed, and the chapter concludes with a discussion of the future directions this research can take.

Suggestions for Further Research

Developing a model is an iterative process, and there is a large scope for further research on the presented model. There are assumptions made at each step of the methodology, some of which are discussed here. Each assumption adds a level of uncertainty to the results of the model and are worth exploring to reduce this level of uncertainty.

There is a potential for additional analysis on the normalization method used to develop a reduced form representation of production temperature for water and CO₂. A geothermal system using CO₂ is in reality a mixed-fluid system because of the initial production of naturally occurring brine within the reservoir. Because breakthrough occurs at different times for different scenarios, it would be interesting to see how this and permeability effect the normalization. Furthermore, it would be beneficial to study an extreme case, increasing the mass flow past 250 kg/s and/or increasing the time of extraction past 200 years, when the temperature of the working fluid reaches the injection temperature, particularly in the case of CO₂. Such an extreme case can reveal how well the fitted curve reflects NUFT simulations.

The natural resource economics approach requires a cost function that depends on the energy that is extracted from the reservoir. Research that determines a function that captures how the cost changes will directly affect the results of the model, particularly when the LCOE is high enough to make it too expensive to extract energy. While this thesis has a larger focus on the reservoir performance, additional work can explore the economics of geothermal power generation from sedimentary basins.

A system dynamics approach, the study of information feedback through causal links, can be used to understand the effects of reservoir parameters on production temperature can expose interconnections between variables. System Dynamics can aid in parameterizing energy that is extracted and heat flow into the reservoir by identifying and highlighting important variables and interactions that affect them. A system dynamics approach may be particularly beneficial when using CO₂ as the geofluid as this system is more complex than water. There are also many assumptions made to maintain simplicity of the model, such as an equal mass flowrate for injection and production well and a homogenous reservoir. But, there is a potential for research to remove these assumptions and add layers of complexity to the model. For example, plant and reservoir efficiency are assumed to be constant. This is not the case in a real power plant that generally loses efficiency as the temperature of the produced fluid decreases. Karvounis (2013) discusses how thermal efficiency of binary

plants operate under conditions similar to geothermal plants, and uses the following equation to calculate the net electrical energy production.

$$\eta = \frac{0.0935 \cdot T_{prod,t} - 2.3266}{100} \quad (23)$$

A changing efficiency, like equation 18, adds an economic cost of temperature drawdown and is likely to change the optimal mass flowrate time path, particularly for scenarios with large temperature drawdown.

Future modeling simulations could investigate the performance of sedimentary basin geothermal reservoirs when the mass flowrates for the injection well(s) and the production well(s) differ, and thus changes in reservoir pressure could affect the performance of the geothermal reservoir. Furthermore, since sedimentary basin geothermal resources do not require faulted and fracture systems, which are localized, and instead use widespread porous and permeable sedimentary layers with presence in states such as Utah, Colorado, and Texas, one could imagine an array of sedimentary basin geothermal facilities, where heat extraction in one location may also drain heat from a neighboring location. Such an externality may have to be negotiated by an institutional process like unitization that occurs in the oil and gas industry, or if all of the neighboring sites are operated by the same utility, lead to an optimal rotation of sites.

Conclusion

Geothermal heat is a renewable resource that can benefit society if it is extracted and used in a cost-effective manner. In a sedimentary basin, heat from the produced fluid is converted to electricity for a profit. Although the temperature of a reservoir will naturally regenerate, extracting heat over long periods of time can drawdown this temperature if the extraction rate exceeds the regeneration rate. As such, this drawdown can limit the long-term performance of the reservoir, while a high rate of heat extraction can produce a large economic gain from selling the energy that is extracted. The model uses a natural resource economics approach to develop a model that determines the optimal extraction strategy given the depreciation of the resource. Results suggest that drawing down the temperature of a reservoir can be the optimal path if the rate at which the natural capital (i.e., heat) grows is less than the rate at which the financial capital (i.e., profit) grows. Though the natural resource economic model is specific to a sedimentary basin using a radial production well and vertical injection well system, the natural resource economic approach and model can be expanded for any type of geothermal resource using the same methodology. Such models can provide economically viable extraction strategies. This will reduce the economic risk associated with the deployment of geothermal resources, the use of which will combat global climate change.

References

- Adams, B.M., Kuehn, T.H., Bielicki, J.M., Randolph, J.B., Saar, M.O., 2015. A Comparison of Electric Power Output of CO₂ Plume Geothermal (CPG) and Brine Geothermal Systems for Varying Reservoir Conditions. *Appl. Energy* 140, 365–377. doi:10.1016/j.apenergy.2014.11.043
- Adams, B.M., Kuehn, T.H., Bielicki, J.M., Randolph, J.B., Saar, M.O., 2014. On the Importance of the Thermosiphon Effect in CPG (CO₂ plume geothermal) Power Systems. *Energy* 69, 409–418. doi:10.1016/j.energy.2014.03.032
- Anderson, T.C., 2013. Geothermal Potential of Deep Sedimentary Basins in the United States. *GRC Trans.* 37.
- Arslan, O., 2010. Exergoeconomic Evaluation of Electricity Generation by the Medium Temperature Geothermal Resources, Using a Kalina Cycle: Simav Case Study. *Int. J. Therm. Sci.* 49, 1866–1873. doi:10.1016/j.ijthermalsci.2010.05.009
- Atrens, A.D., Gurgenci, H., Rudolph, V., 2009. CO₂ Thermosiphon for Competitive Geothermal Power Generation. *Energy and Fuels* 23, 553–557. doi:10.1021/ef800601z
- Axelsson, G., Stefánsson, V., Björnsson, G., 2004. Sustainable Utilization of Geothermal Resources for 100 – 300 Years. Twenty-Ninth Work. *Geotherm. Reserv. Eng.* 9.
- Bertani, R., 2012. Geothermal Power Generation in the World 2005-2010 Update Report.

- Geothermics 41, 1–29. doi:10.1016/j.geothermics.2011.10.001
- Birch, C.P.D., 1999. A New Generalized Logistic Sigmoid Growth Equation Compared with the Richards Growth Equation. *Ann. Bot.* 83, 713–723. doi:10.1006/anbo.1999.0877
- Birkholzer, J., Zhou, Q., Tsang, C., 2009. Large-scale Impact of CO₂ Storage in Deep Saline Aquifers: A Sensitivity Study on Pressure Response in Stratified Systems. *Int. J. Greenh. Gas Control* 3, 181–194. doi:10.1016/j.ijggc.2008.08.002
- Bolin, B., 2007. A History of the Sciences and Politics of Climate Change: The Role of the Intergovernmental Panel on Climate Change. Cambridge Univ. Press 1–11.
- Bonfil, R., 2005. Fishery Stock Assessment Models and their Application to Sharks, in: *Management Techniques for Elasmobranch Fisheries*. pp. 154–181.
- Bowman, C.D., Arthur, E.D., Lisowski, P.W., Lawrence, G.P., Jensen, R.J., Anderson, J.L., Blind, B., Cappiello, M., Davidson, J.W., England, T.R., Engel, L.N., Haight, R.C., Hughes, H.G., Ireland, J.R., Krakowski, R.A., LaBauve, R.J., Letellier, B.C., Perry, R.T., Russell, G.J., Staudhammer, K.P., Versamis, G., Wilson, W.B., 1992. Nuclear Energy Generation and Waste Transmutation Using an Accelerator-driven Intense Thermal Neutron Source. *Nucl. Inst. Methods Phys. Res. A* 320, 336–367. doi:10.1016/0168-9002(92)90795-6
- Bromley, C.J., Mongillo, M., Rybach, L., 2006. Sustainable Utilization Strategies and Promotion of Beneficial Environmental Effects—Having your Cake and Eating it too. *Proc. World Geotherm. Congr.*
- Brown, D., 2000. A Hot Dry Rock Geothermal Energy Concept Utilizing Supercritical CO₂

- Instead of Water. Twenty-Fifth Work. Geotherm. Reservoir Eng. 1995, 1–6.
- Brundtland Commission, 1987. Our common future, Oxford University Press. Oxford.
- Burgess, D.R., 2016. Thermochemical Data, in: NIST Chemistry WebBook, NIST Standard Reference Database Number 69, Eds. P.J. Linstrom and W.G. Mallard. National Institute of Standards and Technology, Gaithersburg, MD.
- Buscheck, T.A., Bielicki, J.M., Edmunds, T.A., Hao, Y., Sun, Y., Randolph, J.B., Saar, M.O., 2016. Multi-Fluid Geo-Energy Systems: Using Geologic CO₂ Storage for Geothermal Energy Production and Grid-Scale Energy Storage in Sedimentary Basins. Geospheres.
- Buscheck, T.A., Chen, M., Lu, C., Sun, Y., Hao, Y., Elliot, T.R., Choi, H., Bielicki, J.M., 2013. Analysis of Operation Strategies for Utilizing CO₂ for Geothermal Energy Production, in: Workshop on Geothermal Reservoir Engineering Stanford University. Stanford, California.
- Buscheck, T.A., Glascoe, L.G., Lee, K.H., Gansemer, J., Sun, Y., Mansoor, K., 2003. Validation of the Multiscale Thermohydrologic Model Used for Analysis of a Proposed Repository at Yucca Mountain. J. Contam. Hydrol. 62-63, 421–440. doi:10.1016/S0169-7722(02)00157-2
- Cacace, M., Kaiser, B.O., Lewerenz, B., Scheck-Wenderoth, M., 2010. Geothermal Energy in Sedimentary Basins: What we can Learn from Regional Numerical Models. Chemie der Erde - Geochemistry 70, 33–46. doi:10.1016/j.chemer.2010.05.017
- Conrad, J.M., 1999. Resource Economics, First. ed. Cambridge University Press, New York.

- de Moor, A., 2001. Towards a Grand Deal on Subsidies and Climate Change. *Nat. Resour. Forum* 25, 167–176. doi:10.1111/j.1477-8947.2001.tb00758.x
- Ewing, R.C., Weber, W.J., Clinard, F.W., 1995. Radiation Effects in Nuclear Waste Forms for High-Level Radioactive Waste. *Prog. Nucl. Energy* 29, 63–127. doi:10.1016/0149-1970(94)00016-Y
- Fenghour, A., Wakeham, W.A., Vesovic, V., 1998. The Viscosity of Carbon Dioxide. *J. Phys. Chem. Ref. Data* 27, 31–44. doi:10.1098/rspa.1912.0058
- Ford, A., 2010. *Modeling the Environment*, 2nd ed. Island Press, Washington D.C.
- Fox, D.B., Sutter, D., Beckers, K.F., Lukawski, M.Z., Koch, D.L., Anderson, B.J., Tester, J.W., 2013. Sustainable Heat Farming: Modeling Extraction and Recovery in Discretely Fractured Geothermal Reservoirs. *Geothermics* 46, 42–54. doi:10.1016/j.geothermics.2012.09.001
- Franco, A., Vaccaro, M., 2012. An Integrated “Reservoir-Plant” Strategy for a Sustainable and Efficient Use of Geothermal Resources. *Energy* 37, 299–310. doi:10.1016/j.energy.2011.11.029
- Fridleifsson, I.B., Bertani, R., Lund, J.W., Rybach, L., 2008. The Possible Role and Contribution of Geothermal Energy to the Mitigation of Climate Change, in: *IPCC Scoping Meeting on Renewable Energy Source*. pp. 59–80.
- Garapati, N., Randolph, J.B., Saar, M.O., 2015. Brine Displacement by CO₂, Energy Extraction Rates, and Lifespan of a CO₂-Limited CO₂-Plume Geothermal (CPG) System with a Horizontal Production Well. *Geothermics* 55, 182–194. doi:10.1016/j.geothermics.2015.02.005

- Garapati, N., Randolph, J.B., Saar, M.O., 2014a. Total Heat Energy Output From, Thermal Energy Contributions To, and Reservoir Development of CO₂ Plume Geothermal (CPG) Systems 1–12.
- Garapati, N., Randolph, J.B., Valencia, J.L., Saar, M.O., 2014b. CO₂-Plume Geothermal (CPG) Heat Extraction in Multi-layered Geologic Reservoirs. *Energy Procedia* 63, 7631–7643. doi:10.1016/j.egypro.2014.11.797
- Goldstein, B., Hiriart, G., Bertani, R., Bromley, C.J., Gutierrez-Negrin, L., Huenges, E., Muroaka, M.A., Ragnarsson, H., Tester, J., 2011. Geothermal Energy, in: Zemedkun, M.T., Wratt, D. (Eds.), *IPCC Special Report on Renewable Energy Sources and Climate Change Mitigation*. Cambridge University Press, Cambridge, UK and New York, NY, USA, pp. 401–436.
- Gordon, H.S., 1954. The Economic Theory of a Common-Property Resource: The Fishery. *J. Polit. Econ.* 62, 124–142.
- Hao, Y., Sun, Y., Nitao, J.J., 2011. Overview of NUFT: Versatile Numerical Model for Simulating Flow and Reactive Transport in Porous Media. *Groundw. React. Transp. Model.* 213–240. doi:10.2174/97816080530631120101
- Holloway, S., 2005. Underground Sequestration of Carbon Dioxide—a Viable Greenhouse Gas Mitigation Option. *Energy* 30, 2318–2333. doi:10.1016/j.energy.2003.10.023
- Hu, F.B., Goldberg, J., Hedeker, D., Flay, B.R., Pentz, M. a, 1998. Comparison of Population-Averaged and Subject-Specific Approaches for Analyzing Repeated Binary Outcomes. *Am. J. Epidemiol.* 147, 694–703. doi:10.1093/oxfordjournals.aje.a009511

- Institute for Energy Reserach, 2015. Geothermal [WWW Document]. Inst. Energy Res.
URL <http://instituteeforenergyresearch.org/topics/encyclopedia/geothermal/> (accessed 1.1.16).
- Johnson, J.W., Nitao, J.J., Morris, J.P., 2005. Modeling the Long-term Isolation Performance of Natural and Engineered Geological CO₂ Storage Sites. Proc. Seventh Int. Conf. Greenh. Gas Control Technol. 5-9 Sept. 2004, Vancouver, Canada 2, 1315–1321. doi:10.1016/B978-008044704-9/50144-0
- Johnston, I.W., Narsilio, G. a., Colls, S., 2011. Emerging Geothermal Energy Technologies. KSCE J. Civ. Eng. 15, 643–653. doi:10.1007/s12205-011-0005-7
- Karvounis, D.C., 2013. Simulations of Enhanced Geothermal Systems with an Adaptive Hierarchical Fracture Representation. doi:10.3929/ethz-a-009967366
- Kose, R., 2007. Geothermal Energy Potential for Power Generation in Turkey: A Case Study in Simav, Kutahya. Renew. Sustain. Energy Rev. 11, 497–511. doi:10.1016/j.rser.2005.03.005
- Ledingham, P., 1998. The World Directory of Renewable Energy: Suppliers and Services. Geotherm. Energy 29, 108–110.
- Lei, Y.C., Zhang, S.Y., 2004. Features and Partial Derivatives of Bertalanffy-Richards Growth Model in Forestry. Nonlinear Anal. Model. Control 9, 65–73.
- Mansoor, K., Carroll, S.A., Sun, Y., 2015. The Role of Wellbore Remediation on the Evolution of Groundwater Quality from CO₂ and Brine Leakage. Energy Procedia 68, 1–8. doi:10.1016/j.egypro.2014.11.510
- Mitra, T., Wan, H.Y., 1986. On the Faustmann Solution to the Forest Management

- Problem. *J. Econ. Theory* 40, 229–249. doi:10.1016/0022-0531(86)90073-6
- Murphy, H., Niitsuma, H., 1999. Strategies for Compensating for Higher Costs of Geothermal Electricity with Environmental Benefits. *Geothermics* 28, 693–711. doi:http://dx.doi.org/10.1016/S0375-6505(99)00018-8
- Nitao, J.J., Martins, S.A., Ridley, M.N., 2000. Field Validation of the NUFT Code for Subsurface Remediation by Soil Vapor Extraction. Livermore, CA.
- Nitao, J.J., Sun, Y., 2015. USNT Reference Manual of the NUFT Code for Yucca Mountain Project. Livermore, CA.
- NOAA National Centers for Environmental Information, 2015. Global Analysis for Annual 2014.
- O’Sullivan, M., Yeh, A., Mannington, W., 2010. Renewability of Geothermal Resources. *Geothermics* 39, 314–320. doi:10.1016/j.geothermics.2010.09.003
- Olasolo, P., Juárez, M.C., Morales, M.P., Damico, S., Liarte, I.A., 2016. Enhanced Geothermal Systems (EGS): A Review. *Renew. Sustain. Energy Rev.* 56, 133–144. doi:10.1016/j.rser.2015.11.031
- Ouyang, L.-B., 2011. New Correlations for Predicting the Density and Viscosity of Supercritical Carbon Dioxide. *Open Pet. Eng. J.* 4, 13–21. doi:10.2174/1874834101104010013
- Pistone, S., Horne, R., 2011. The Significance of CO₂ Solubility in Deep Subsurface Environments. Stanford University.
- Randolph, J.B., Saar, M.O., 2011. Combining Geothermal Energy Capture with Geologic Carbon Dioxide Sequestration. *Geophys. Res. Lett.* 38, 1–7.

doi:10.1029/2011GL047265

- Rechar, R.P., Lee, J.H., Hardin, E.L., Bryan, C.R., 2014. Waste Package Degradation from Thermal and Chemical Processes in Performance Assessments for the Yucca Mountain Disposal System for Spent Nuclear Fuel and High-level Radioactive Waste. *Reliab. Eng. Syst. Saf.* 122, 145–164. doi:10.1016/j.res.2013.06.030
- Richards, F.J., 1959. A Flexible Growth Constant for Empirical Use. *J. Exp. Bot.* 10, 290–300.
- Rybach, L., 2007. Geothermal Sustainability, in: *European Geothermal Congress*. Zurich, Switzerland, pp. 1–7.
- Rybach, L., 2003. Geothermal Energy: Sustainability and the Environment. *Geothermics* 32, 463–470. doi:10.1016/S0375-6505(03)00057-9
- Rybach, L., Megel, T., Eugster, W.J., 2000. At What Time Scale are Geothermal Resources Renewable? *Proc. World Geotherm. Congr. 2000 Kyushu-Tohoku, Japan* 867–872.
- Saar, M.O., Buscheck, T.A., Jenny, P., Garapati, N., Randolph, J.B., Karvounis, D.C., Chen, M., Sun, Y., Bielicki, J.M., 2015. Numerical Study of Multi-Fluid and Multi-Level Geothermal System Performance. *Proceedings, World Geotherm. Congr. 2015*.
- Sahni, A., Kumar, M., Knapp, R.B., 2000. Electromagnetic Heating Methods for Heavy Oil Reservoirs, *SPE/AAPG Western Regional Meeting*. Livermore, CA. doi:10.2118/62550-MS
- Sanyal, S.K., 2005. Sustainability and Renewability of Geothermal Power Capacity. *Geotherm. Energy* 24–29.
- Sanyal, S.K., 2004. Cost of Geothermal Power and Factors that Affect it. *Proc. 29th Work.*

- Geotherm. Reserv. Eng. 26–28.
- Sanyal, S.K., Morrow, J.W., Butler, S.J., Robertson-tait, A., 2007. Cost of Electricity from Enhanced Geothermal Systems, in: Thirty-Second Workshop on Geothermal Reservoir Engineering. p. 11.
- Sawyer, J.S., 1972. Man-made Carbon Dioxide and the “Greenhouse Effect.” *Nature* 239, 23–26. doi:10.1038/239023a0
- Sovacool, B.K., 2008. Valuing the Greenhouse Gas Emissions from Nuclear Power: A Critical Survey. *Energy Policy* 36, 2940–2953. doi:10.1016/j.enpol.2008.04.017
- Span, R., Wagner, W., 1996. A New Equation of State for Carbon Dioxide Covering the Fluid Region from the Triple-point Temperature to 1100K at Pressure up to 800MPa. *J. Phys. Chem. Ref. Data* 25, 1509–1596.
- Stefansson, V., 2000. The Renewability of Geothermal Energy. *World Geotherm. Congr.* 883–888.
- Stefánsson, V., 2002. Investment Cost for Geothermal Power Plants. *Geothermics* 31, 263–272. doi:10.1016/S0375-6505(01)00018-9
- Sterman, J.D., 2000. *Business Dynamics: Systems Thinking and Modeling for a Complex World*. Jeffrey J. Shelstad, Massachusetts Institute of Technology, Cambridge, MA.
- Sun, Y., Demir, Z., Delorenzo, T., Nitao, J.J., 2000. Application of the NUFT Code for Subsurface Remediation by Bioventing. Livermore, CA.
- Tahvonen, O., Pukkala, T., Laiho, O., Lähde, E., Niinimäki, S., 2010. Optimal Management of Uneven-Aged Norway Spruce Stands. *For. Ecol. Manage.* 260, 106–115. doi:10.1016/j.foreco.2010.04.006

- United Nations, 2015. Adoption of the Paris Agreement, in: Framework Convention on Climate Change. Paris, France, pp. 1–32.
- Walker, G., 1995. Energy, Land Use and Renewables: A Changing Agenda. Land use policy 12, 3–6. doi:10.1016/0264-8377(95)90069-E
- WEC, 1998. Survey of Energy Resources, in: World Energy Council. London, p. 294.
- Weitzman, M., 2003. Income, Wealth, and the Maximum Principle. Cambridge: Harvard University Press.
- Xu, R., Zhang, L., Zhang, F., Jiang, P., 2015. A Review on Heat Transfer and Energy Conversion in the Enhanced Geothermal Systems with Water/CO₂ as Working Fluid. Int. J. Energy Res. 39, 1722–1741. doi:10.1002/er.3352

Appendix A: Nomenclature

Variable	Description	Units
T_{prod}	Temperature of production fluid	K
$T_{t=0}$	Initial temperature of the reservoir	K
T_{inj}	Injection temperature of fluid	K
Ξ	Present value of net benefits	\$
ξ	Net profit per unit of extracted energy	\$/kJ
p	Selling price of electricity	\$/kJ
$C_{t=0}$	Investment cost	\$
η	Power plant and wellbore efficiency factor	%
δ	Discount rate	%
L, A, x, M, v	Logistic curve regression coefficients	-
t	Time	s
Δt	Time step	s
Ω	Planning horizon	years
ω	Total number of decision periods	-
s	Current decision period	-
τ_s	Time elapsed at the end of current decision period	years
$\Delta \tau$	Time of decision period	years
k	Thermal conductivity	W/m-K
ρ	Density	kg/m ³
c_p	Specific heat capacity	kJ/(K-kg)
β	Compressibility	Pa ⁻¹

G	Temperature gradient	K/km
T_s	Temperature of the surface	K
z	Reservoir depth from surface	m
Δz	Reservoir thickness	m
r	Distance from injection well to production well	m
κ	Permeability	m^2
ϕ	Porosity	-
Q_t	Energy that is extracted	kJ
Q_{tot}	Total energy that could have been extracted	kJ
$Q_{res,t=0}$	Initial energy in reservoir at $t=0$	kJ
Q_{in}	Net energy entering the reservoir	kJ
\dot{m}	Mass flow rate	kg/s
\bar{Q}	Normalized energy extracted	-
\bar{T}	Normalized production temperature	-

Appendix B: Programming Code

The following code is for developing the normalization figures with a fitted curve for water. A duplicate code was used for the data using CO₂ (MATLab).

```
% LOGISTIC CURVE DATA FIT
% The following code calculates the normalized production
temperature and
% normalized energy extracts, plots it, and fits the
generalized logistic
% curve to the data.

close all
%% Radial Well with Brine Injection %%

radius = 700; %distance b/w injection and production well
poro = 0.1; %porosity
k_rock = 2; %W/m-C
cp_rock = 2.8; %kJ/kg-C
rho_rock = 920; %kg/m^3

Tempinj %reads the injection temperature from the
T_inj_history file
FluxCalc
ReadRuns

%% Read temperature from history files %%
File = dir(fullfile('Radial Well Brine','*')); %list all
contents in Radial Well Folder
numF = length(File); %number of content in the Radial
Well Folder
cd('Radial Well Brine') % change current folder to Radial
Well
% legen = {};
QFall = [];
TFall = [];

for i = 1:numF % loop for all the files in Radial Well
Folder
    if (File(i).isdir == 0) % if content is a file
        A = File(i).name;
        [time,T] = textread(File(i).name,'%f
%f','headerlines',11); %read in prod temp data
```

```

        a = regexp(A, 'Run', 'split'); b =
regexp(a{2}, '.T', 'split'); %Reading run number from file
name
        Run = str2double(b{1});
%         legen = vertcat(legen, {strcat('Run
', [num2str(Run, '%2.0i')])});
        T_initial = max(T); % initial temperature of
production well
        T_bottom = 15 +
(Tgrad(Run)/1000)*(depth(Run)+thickness(Run));
        %% depth specific fluid characteristics
        if depth(Run)==2500
            cp_brine = 4.16; %kJ/kg-C
            rho_brine = 954; %kg/m^3
        elseif depth(Run)==3500
            cp_brine = 4.18; %kJ/kg-C
            rho_brine = 928; %kg/m^3
        elseif depth(Run)==5000
            cp_brine = 4.23; %kJ/kg-C
            rho_brine = 864; %kg/m^3
        end
        %% Calculate TF
        TempF = (T - Tinj(Run))/(T_initial - Tinj(Run));
%temperature fraction
        Vol = thickness(Run)*pi*(radius^2);
        %% Initialize variables
        QF = zeros(size(TempF));
        Q_total = zeros(size(TempF));
        Ecum = zeros(size(TempF));
        F_total_c = squeeze(F_total(:,Run));
        F_total_r = F_total_c(F_total_c~=0);
        if length(TempF) ~= length(F_total_r)
            F_flow = zeros(size(TempF));
            F_flow(2:end) = F_total_r;
        else
            F_flow = F_total_r;
        end
        F_in = zeros(size(TempF));
        Flow = zeros(size(TempF));
        Qex = zeros(size(TempF));
        Q_stored = (Vol*(1-
poro)*rho_rock*cp_rock*(T_initial)) +
(Vol*poro*rho_brine*cp_brine*(T_initial)); % [kJ]
        Q_total(1) = Q_stored;
        Qex(1)=0;

```

```

%% Calculate QF
for k = 2:length(T)
    F_in(k) = F_in(k-1) + (F_flow(k)*(time(k)-
time(k-1)))/1000; %kJ
    Flow(k) = (F_flow(k)*(time(k)-time(k-1)))/1000;
    Ecum(k) = (mrate(Run)*cp_brine*(T(k)-
Tinj(Run))*(time(k)-time(k-1))); %kJ
    Qex(k) = Qex(k-1) + Ecum(k);
    Q_total(k) = Q_stored + F_in(k)+Qex(k);
    QF(k) = Qex(k)/Q_total(k);
end
QFall = vertcat(QFall,QF);
TFall = vertcat(TFall,TempF);
%% Plot Data
hold on
plot(QF,TempF,'ko-')%, 'MarkerEdgeColor',[0.5 0.5
0.5], 'Color',[0.5 0.5 0.5])
% end
end
end
% legend(legend)
axis([0 1 0 1])
cd ..
%% LOGISTIC CURVE
LowerBound = [0 0 0 0 0];
UpperBound = [Inf Inf Inf Inf Inf];
Seed = [1 1 1 1 1];
ft = fittype('LogisticFit( x, alpha, beta, k, M, m)');
[FO,GOF] =
fit(QFall,TFall,ft,'Lower',LowerBound,'Upper',UpperBound,'S
tartPoint',Seed);
h = plot(FO); set(h,'LineWidth',2);
parameters = coeffnames(FO); values = coeffvalues(FO);
startx = 0.1; starty = 0.4; ad =
ones(1,numel(parameters))*0.04;
text(startx,starty,['y = LogisticFit']);
text(startx,starty,['y = ' formula(FO)]);

for idx = 1:numel(parameters)
    text(startx,starty-
(ad(idx)*idx),strcat(parameters(idx), {' = '},
num2str(values(idx))));
end
text(startx,starty-sum(ad)-ad(1),strcat({'r^2 = '},
num2str(GOF.rsquare)));

```

```
title('Radial Well; Geofluid: Water; Depth: 3500m')
xlabel('Normalized Energy Extracted [dim]')
ylabel('Normalized Production Temperature [dim]')
```

The following code is for the separated code and functions used the normalization code

(MATLab).

```
% Read injection temperature for every run

cd('Radial Well Brine')
File = dir(fullfile('T_inj_history','*')); %list all
contents in Radial Well Folder
numF = length(File); %number of content in the Radial
Well Folder
cd('T_inj_history') % change current folder to Radial
Well
Tinj = zeros(size(numF-2));
for i=1:numF
    if (File(i).isdir == 0) % if content is a file
        A = File(i).name;
        a = regexp(A, 'Run', 'split'); b =
regexp(a{2}, '.T', 'split'); %Reading run number from file
name
        Run = str2double(b{1});
        [time,T_injread] = textread(File(i).name, '%f
%f', 'headerlines', 10);
        Tinj(Run) = min(T_injread);
    end
end
cd ..
cd ..
```

```
close all
tic
ReadRuns

%looking at flux files
```

```

File = dir(fullfile('Radial Well Brine Flux','*')); %list
all contents in Folder
numF = length(File); %number of content in Folder
cd('Radial Well Brine Flux') % change current folder
%% Hard coded numbers
tstep = 250;
numsim = 300;
F_top = zeros(tstep,23,numsim);
F_bottom = zeros(tstep,23,numsim);
F_side = zeros(tstep,11,numsim);
% Tprod = zeros(a,numsim);
time_run = zeros(tstep,numsim);
% Ecum = zeros(a,numsim);
%% Put Data into matrices
for i = 1:numF %loop over all files
    if (File(i).isdir == 0) % if content is a file
        A = File(i).name;
        a = regexp(A, '_', 'split');
        b = regexp(a{3}, '.Cond', 'split');
        bb=regexp(b{1}, 'Run', 'split');%Reading run number from file
        name
        Run = str2double(bb{2});
        xLoc = str2double(a{4});
        if (size(b{2},2) == size('top',2))
            if (b{2} == 'top')
                [t1,F] = textread(File(i).name,'%f
%f','headerlines',13); %read in prod temp data
                len = length(F);
                F_top(1:len,xLoc,Run) = F;
            end
        elseif (size(b{2},2) == size('bottom',2))
            if (b{2} == 'bottom')
                [t1,F] = textread(File(i).name,'%f
%f','headerlines',13); %read in prod temp data
                len = length(F);
                F_bottom(1:len,xLoc,Run) = F;
            end
        elseif (size(b{2},2) == size('side',2))
            if (b{2} == 'side')
                [t1,F] = textread(File(i).name,'%f
%f','headerlines',13); %read in prod temp data
                len = length(F);
                F_side(1:len,xLoc,Run) = F;
            end
        end
    end
end
end

```

```

        time_run(1:len,Run) = t1;
    end
end

%% Sum data for each run
[t,xdir,Runsim] = size(F_top);
F_total = zeros(t,Runsim);
fluxsumtop = 0;
fluxsumbottom = 0;
fluxsumside =0;
for k = 1:Runsim
    Ftoprun = sum(squeeze(F_top(:,:,k)),2);
    Fbotrun = sum(squeeze(F_bottom(:,:,k)),2);
    Fsidrun = sum(squeeze(F_side(:,:,k)),2);
    F_total(:,k) = Ftoprun + Fbotrun + Fsidrun;
end
cd ..

%% Injection temperature
File = dir(fullfile('R Brine Flux Inj T','*')); %list all
contents in Folder
numF = length(File);
cd('R Brine Flux Inj T') % change current folder to
Radial Well
Tinj = zeros(100,1);
for i=1:numF
    if (File(i).isdir == 0) % if content is a file
        A = File(i).name;
        a = regexp(A,'Run','split'); b =
regexp(a{2},'.T','split'); %Reading run number from file
name
        Run = str2double(b{1});
        [time,T_injread] = textread(File(i).name,'%f
%f','headerlines',11);
        Tinj(Run) =mean(T_injread(20:end));
    end
end
cd ..

%% Production temperature and Energy extracted
File = dir(fullfile('R Brine Flux Prod T','*')); %list all
contents in Folder
numF = length(File);
cd('R Brine Flux Prod T') % change current folder to
Radial Well

```

```

for i=1:numF
    if (File(i).isdir == 0) % if content is a file
        A = File(i).name;
        a = regexp(A, 'Run', 'split'); b =
regexp(a{2}, '.T', 'split'); %Reading run number from file
name
        Run = str2double(b{1});
        [time,T_prodread] = textread(File(i).name, '%f
%f', 'headerlines', 11);
        len = length(T_prodread);
        Tprod(1:len,Run) = T_prodread;
        %
        time_run(1:len,Run) = time;
        if depth(Run)==2500
            cp_brine = 4.2; %kJ/kg-C
        elseif depth(Run)==3500
            cp_brine = 4.3; %kJ/kg-C
        elseif depth(Run)==5000
            cp_brine = 4.4; %kJ/kg-C
        end
        Es = zeros(1,length(time));
        for k = 2:length(time)
            Es(k) = Es(k-
1)+(mrate(Run)*cp_brine*(T_prodread(k)-Tinj(Run))*(time(k)-
time(k-1)));
        end
        Ecum(1:len,Run) = Es;
    end
end
cd ..

```

```

% read from Runs Tracker

```

```

% Read Excel Sheet with Run Data
Perm = xlsread('Runs Tracker','Radial Well
Brine','C2:C301'); % Permeability of run [m^2]
depth = xlsread('Runs Tracker','Radial Well
Brine','D2:D301'); %depth [m]
Tgrad = xlsread('Runs Tracker','Radial Well
Brine','E2:E301'); %temperature gradient [C/km]
thickness = xlsread('Runs Tracker','Radial Well
Brine','F2:F301'); % thickness of reservoir
[m]

```

```

mrate = xlsread('Runs Tracker','Radial Well
Brine','G2:G301');           % mass flowrate [kg/s]

```

```

function [ y ] = LogisticFit( x, alpha, beta, k, M, m )
%LogisticFit is a curve fitting for a Generalied Logistic
Function
%   Written by Iti Patel

y = zeros(size(x));

for i = 1:length(x)
    y(i) = 1 + (alpha-1) / ( ( 1 + beta*exp(-k*(x(i)-M))
)^ (1/m) ) ;
end

end

```

The following code is for the STATA regression analysis (.do file).

```

clear

cd "C:\Users\patel.1166\Documents\STATA"
use "Data for STATA Water.dta"

rename Permeabilitym2 k
rename Depthm z
rename TemperatureGradientCkm G
rename Thicknessm dz
rename MassFlowratekgs mr
rename Times t
rename QinkJ Qin
rename ΣQexkJ CQex
rename QexkJ Qex
rename QstoredkJ Qs

gen b1 = ln(k)
gen b2 = ln(z)
gen b3 = ln(dz)

```

```
gen b4 = ln(mr)
gen b5 = ln(G)
gen b6 = ln(CQex)
gen b7 = ln(Qex)
gen b8 = ln(t)
gen b9 = ln(Qs)
gen ln_Qin = ln(Qin)
```

```
xtset RunID
```

```
xtreg ln_Qin b1 b2 b3 b4 b5 b6 b7 b8 b9, mle nocon
outreg2 using QinRegression, excel replace
```